Tumor-Associated CD19⁺CD39⁻ B Regulatory Cells Deregulate Class-Switch Recombination to Suppress Antibody Responses

Subhadip Pati[1], Sumon Mukherjee[1], Saikat Dutta[1], Aharna Guin[1], Dia Roy[1], Sayantan Bose[1], Silpita Paul[1], Sudipto Saha[2], Sankar Bhattacharyya[3], Pratyush Datta[4], Jayati Chakraborty[4], Diptendra K. Sarkar[5], and Gaurisankar Sa[1]

ABSTRACT

B cells are an essential component of humoral immunity. Their primary function is to mount antigen-specific antibody responses to eliminate pathogens. Despite an increase in B-cell number, we found that serum-IgG levels were low in patients with breast cancer. To solve this conundrum, we used high-dimensional flow cytometry to analyze the heterogeneity of B-cell populations and identified a tumor-specific CD19⁺CD24^hiCD38^hi IL10-producing B regulatory (Breg)-cell subset. Although IL10 is a Breg-cell marker, being an intracellular protein, it is of limited value for Breg-cell isolation. Highly expressed Breg-cell surface proteins CD24 and CD38 also impede the isolation of viable Breg cells. These are hurdles that limit understanding of Breg-cell functions. Our transcriptomic analysis identified, CD39-negativity as an exclusive, sorting-friendly surface marker for tumor-associated Breg cells. We found that the identified CD19⁺CD39⁻IL10⁺ B-cell population

was suppressive in nature as it limited T helper–cell proliferation, type-1 cytokine production, and T effector–cell survival, and augmented CD4⁺FOXP3⁺ regulatory T–cell generation. These tumor-associated Breg cells were also found to restrict autologous T follicular helper–cell expansion and IL21 secretion, thereby inhibiting germinal transcript formation and activation-induced cytidine deaminase expression involved in H-chain class-switch recombination (CSR). This isotype-switching abnormality was shown to hinder B-cell differentiation into class-switched memory B cells and subsequent high-affinity antibody-producing plasma B cells, which collectively led to the dampening of IgG-mediated antibody responses in patients with cancer. As low IgG is associated with poor prognosis in patients with cancer, Breg-cell depletion could be a promising future therapy for boosting plasma B cell–mediated antibody responses.

Introduction

In the immune system, B cells are an essential component of humoral immunity. They are classically positive modulators that regulate inflammation and immune responses. Solid tumors often contain B-cell populations, suggesting B cells have a role in influencing the tumor microenvironment alone or in cooperation with other resident cells (1, 2). The role of B cells in cancer is equivocal. On one hand, B cells are thought to be the immune system's defensive powerhouse as they secrete antibodies and build up a memory B cell–mediated immune response against tumors (3). On the other hand, tumors show a reduction in metastasis following CD20 depletion from the total B-cell pool (4, 5). Further research led to the identification of a new pro-tumor B-cell branch with a suppressive function that exists alongside the well-known antitumoral B-cell subsets like memory and plasma B cells. The newly observed immu-

nosuppressive B cells were later designated as B regulatory (Breg) cells (6, 7).

Despite reaching a partial consensus on the IL10-mediated effector function of Breg cells, the field has yet to produce a unified view on the phenotypic status of Breg cells (8, 9). Several IL10-producing Breg-cell subsets with different surface markers have been described so far. Among them, CD19⁺CD24^hiCD38^hi B cells have a phenotype associated with transitional B cells (10), and CD19⁺CD24^hiCD27⁺, a phenotype associated with memory B cells (11), make up the majority of IL10-secreting Breg cells. It is now widely accepted that Breg cells perform immunoregulatory functions primarily through the secretion of cytokines such as IL10, IL35, and TGFβ as well as other proteins such as granzyme-B and programmed death-ligand 1 (PD-L1; refs. 7, 12, 13). Although the presence of suppressive B cells in various autoimmune disorders has been known for more than 30 years (14), very little is known about their presence and function in the field of tumor biology. Breg cells appear to suppress T helper cells, induce FOXP3⁺ regulatory T (Treg) cells, and target other tumor-infiltrating lymphocytes such as myeloid-derived suppressor cells, macrophages, and natural killer cells to thwart antitumor immunity (15, 16). Various studies have also shown that Breg cells are closely associated with many clinicopathologic factors in patients with solid tumors and may be potential biomarkers for predicting patient survival (14). A study on gastric cancer found that Breg cells suppress the immune system by downregulating Th1 cells and increasing Treg-cell generation (17, 18). These findings suggest the potential for therapeutic targeting of Breg cells in patients with cancer. Breg cells are widely known to be immunosuppressive B-cell subsets. However, other than intracellular IL10, no phenotypic surface signature has yet been assigned to this B-cell subset in the tumor microenvironment.

[1]Division of Molecular Medicine, Bose Institute, Calcutta Improvement Trust Scheme VII M, Kolkata, West Bengal, India. [2]Division of Bioinformatics, Bose Institute, Calcutta Improvement Trust Scheme VII M, Kolkata, West Bengal, India. [3]Immunobiology and Translational Medicine Laboratory, Department of Zoology, Sidho Kanho Birsha University, Purulia, West Bengal, India. [4]Department of Pathology, ESI-PGIMSR, Medical College Hospital and ODC (EZ), Kolkata, West Bengal, India. [5]Department of Surgery, IPGMER-SSKM Hospital, 244, AJC Bose Road, Kolkata, West Bengal, India.

Corresponding Author: Gaurisankar Sa, Division of Molecular Medicine, Bose Institute, P-1/12 CIT Scheme VII M, Kolkata, West Bengal 700054, India. Phone: 332-569-3147; E-mail: gauri@jcbose.ac.in

In this study, using high-dimensional flow-cytometric and transcriptomic analysis, we identified a phenotypic signature for tumor-associated IL10-producing Breg cells, which can be used to live-sort these cells. Our *ex vivo* findings indicated that, in addition to their T cell–mediated immunoregulatory function, Breg cells play an important role in limiting the production of germline transcripts (GLT), activation-induced cytidine deaminase (AID) expression involved in class-switching recombination (CSR), B-cell differentiation, and antibody production in the tumor microenvironment.

Materials and Methods

Patients and controls

Patients with breast cancer ($n = 45$; females, age 18–64 years), classified as invasive carcinoma of no special type (ductal), were enrolled in the study. Fifteen age-/sex-matched healthy individuals (aged 22–62 years), 8 patients with rheumatoid arthritis (RA), and 6 HBV-infected patients were studied in parallel as controls. Blood and tissue samples were obtained between August 2017 and September 2022. Tissues from primary breast tumor lesions were collected from patients undergoing surgical procedures. In all cases, research personnel obtained and processed tissue within 1 hour of surgery. All the freshly collected tissues and bloods were processed immediately. In an unbiased way, patients with RA who had a moderate to high disease activity index and did not have any other systemic diseases were included in the study. The ethical approval for the collection of postoperative breast tumor tissue samples and peripheral blood from patients with breast cancer, patients with RA, and healthy individuals and subsequent experiments with them for this study was sanctioned under the provisions of the ethics committee, ESI Post-Graduate Institute of Medical Science and Research, Kolkata, India (Approval no: ESI-PGIMSR/MKT/IEC/13/2017), the Institute of Post-Graduate Medical Education and Research Oversight Committee (Approval no. IPGME&R/IEC/2018/643) and the Human Ethics Committee, Bose Institute (Approval no: BIHEC/2017–18/7). Informed written consent was obtained from all patients enrolled in the study in compliance with the Declaration of Helsinki. Patient characteristics are in Supplementary Tables S1–S3. Healthy individuals' data are also added in Supplementary Table S4.

Immune subset isolation

Collected peripheral blood was layered over a lymphocyte separation medium (HiSep, Himedia, catalog no. LS001) in a 1:1 ratio. Then a density gradient centrifugation was performed at 1,000 rpm for 40 minutes at room temperature. The buffy coat was then collected, and the cells washed with PBS and resuspended to obtain total leukocytes. Naïve T cells were isolated using a naïve T-cell isolation kit (BioLegend, catalog no. 480041). After obtaining leukocytes, 10 μL of the biotin-antibody cocktail was added to 10^7 cells. After thorough mixing, the cells were incubated on ice for 15 minutes. Then, 10 μL of streptavidin nanobeads were added, mixed well, and incubated on ice for 15 minutes. The cells were then treated with 2.5 mL of PBS before being transferred to a 5 mL (12 × 75 mm) polypropylene tube and placed in the BD cell separation magnet (BD Biosciences, catalog no. 552311) for 5 minutes. The unbound portion of the sample containing the desired naïve CD4$^+$ T cells was then collected. Flow cytometry was used to determine the purity of the sample. CD19$^+$ B cells were isolated using a B-cell enrichment cocktail (BD Biosciences, catalog no. 558007). Five-microliter biotinylated human B lymphocyte enrichment cocktail was added for every $1×10^6$ cells, mixed well by pipetting and incubated for 15 minutes at room temperature. After that, the labelled cells were washed with 10× excess volume of 1× BD IMag buffer (BD Biosciences, catalog no. 552362), centrifuged at $300 × g$ for 7 minutes and the supernatant aspirated. The cells were resuspended in 100 μL of BD IMag buffer before we added 5 μL of BD IMag streptavidin particle, and incubated for 30 minutes at room temperature. Next, we transferred the sample to a 12×75 mm round-bottom test tube and placed the tube on the BD cell separation magnet for 8 minutes. After that, we collected the unbound fraction of the sample containing the desired CD19$^+$ B cells. The purity of enriched cells was determined by flow cytometry and was consistently > 90%. Some of the CD19$^+$ B cells were further separated on the basis of CD39 expression using biotin mouse anti-human CD39 (BioLegend, catalog no. 328204), yielding, CD19$^+$CD39$^-$ Breg cells and CD19$^+$CD39$^-$ Breg-depleted peripheral blood mononuclear cells (PBMC

Cell culture

Isolated cells were cultured in RPMI1640 containing L-glutamine and NAHCO3 (Sigma-Aldrich, catalog no. R8758) supplemented with 25 mmol/L HEPES (Sigma-Aldrich, catalog no. H4034) and 10% FBS (Thermo Fisher Scientific, catalog no. 16000069), and penicillin–streptomycin (Thermo Fisher Scientific, catalog no. 15140122). Isolated naïve T cells were activated with anti-CD3/anti-CD28 (BioLegend, catalog nos. 317302 and 302902, respectively). First, we prepared a 10 μg/mL solution of anti-CD3 and anti-CD28 in sterile PBS. Then, 50μL of the anti-CD3 solution was applied to each microwell of the 96-well test plate and incubated at 37°C for two hours. After washing, we added 200 μL of naïve T-cell suspension (RPMI medium with 10% FBS; $2×10^5$ cells) and 50 μL of anti-CD28 to each well and incubated for 72 hours at 37°C. Recombinant human IL6 (PeproTech, catalog no. 200–06; 25 ng/mL) and IL21 (PeproTech, catalog no. 200–21; 10 ng/mL) were added in the naïve T-cell cultures ($2×10^5$ cells) for 72 hours in the presence with anti-CD3/anti-CD28 to polarize T follicular helper (Tfh) cell. CD19$^+$ B cells ($5×10^5$ cells) were activated for 72 hours with 1 μg/mL recombinant CD40LG (Sino Biological, catalog no. 10239-HO8E-250). For the induction of the memory/plasma phenotype and germinal transcript detection, cells were stimulated for 7 days with CD40LG+IL2 (PeproTech, catalog no. 200–02) +IL4 (PeproTech, catalog no. 200–04) to develop a memory phenotype, CD40LG+IL2+IL10 (IL10, PeproTech, catalog no. 200–10) to develop plasma cells, and CD40LG+IL4+IL10 for GLT detection. Concentrations used for recombinant proteins were CD40LG (1 μg/mL), IL4 (40 ng/mL), IL10 (50 ng/mL), and IL2 (25 ng/mL). To check Breg-cell stability, sorted and unsorted Breg cells from tumor PBMC's were activated with CD40LG (1 μg/mL) in presence of LPS (20 μg /mL; Sigma-Aldrich, L2630) for 7 days. For adenosine-mediated AID production, $5×10^5$ CD19$^+$ B cells from the tumor patient's blood were cultured with CD40LG (1 μg/mL) and adenosine (20 μmol/L; Himedia, catalog no. TC083–5G) for 7 days.

Flow cytometry

Flow cytometry was performed using fluorochrome-conjugated antibodies specific for the following human markers: CD19-BB515/-FITC/-APC/Percp-Cy5.5, CD24-PE-Cy7, CD38-APC, IgM-V500, IgD-APC-Cy7, PD1-Percp-Cy5.5, CD27-PE, IL10-PE/-BV421, CD39-BV421, TGFβ-BV421, CD138-Percp-Cy5.5, IFNγ-PE, Ki67-BV421, IL21-BV421/PE, CXCR5-PE-Cy7/APC, CD4-APC-H7/FITC, CD25-PE-Cy7, FOXP3-APC, Annexin-V-FITC/APC, 7AAD, FOXP3-APC, and CD45-PE. All antibody details can be found in Supplementary Table S5. For multicolor flow-cytometric surface staining, cells were stained at 4°C for 30 minutes. For analysis of intracellular FOXP3 and Ki67, cells were fixed and permeabilized with

transcription factor buffer (BD Biosciences, catalog no. 562574). For detection of the intracellular cytokines IL10 and IFNγ and IL21, cells were stimulated with a cell activation cocktail (PMA and ionomycin) in the presence of brefeldin-A (BioLegend, catalog no. 423304) for the last 5 hours at 37°C. Then the cells were washed, fixed, permeabilized using cytofix and cytoperm buffer set (BD Biosciences, catalog no. 554714), and stained with anti–IFNγ-PE, anti–IL21-BV421 and anti–IL10-PE/-BV421 (see Supplementary Table S5 for details) for 30 minutes using the manufacturer's protocol. Appropriate isotype controls and fluorescence minus one (FMO) were used to set the gates for cytokine detection. CD4$^+$ T-cell apoptosis was evaluated by flow cytometry using 7AAD (BD Biosciences, catalog no. 559925). BD FACS Verse was used to acquire the data and BD FACS Verse Suite software (BD Biosciences), and FlowJo software (BD Biosciences, version 10.0) were used to analyze all flow-cytometry data. For quantifying stained cells in contour plots, dot plots, and quadrants, lines were drawn on the basis of the signals using FMO and unstained controls. For high-dimensional data analysis, t-distributed stochastic neighbor embedding (t-SNE), FlowSOM, and UMAP plugins are used using FlowJo v.10 online guidelines.

Confocal microscopy

For confocal microscopy, isolated CD19$^+$ B cells were treated and stimulated with a cell activation cocktail with brefeldin-A (BioLegend, catalog no. 423304) for 5 hours at 37°C. Then 200 μL of cell suspension (4×10^4 cells) was applied to the poly-L-lysine-coated coverslip and allowed to adhere for 40 to 60 minutes at 37°C. Fixation was performed using 4% paraformaldehyde for 20 minutes at room temperature, followed by permeabilization with cold-methanol for 8 minutes at −20°C. After blocking with 4% BSA (30 minutes), the cells were incubated with anti–human-CD19 (Biotenylated-Ab, BioLegend, catalog no. 302204), anti–IL10 (rabbit-mAb, Cell Signaling Technology, catalog no. 12163S), followed by fluorescence-tagged streptavidin particle (FITC-Streptavidin, BioLegend, catalog no. 405202) and secondary antibodies (BioLegend, catalog no. 406418 and Invitrogen, catalog nos. A11034, A11010, and A11003) for 45 minutes, and DAPI (Sigma, catalog no. 28718–90–3) was added for the last 15 minutes. The cells were examined under a Leica confocal microscope at 63× magnification using DPX2 mounting medium. Images were analyzed by ImageJ software (version 1.53k).

ELISA assay

Cell supernatants from 72-hour culture of Breg and non-Breg cells were harvested and analyzed for IL10 (Ray Biotech, catalog no. ELH-IL10). Cell supernatants from differentiated naïve T cells to Tfh cells were harvested at different time points and monitored by ELISA for IL21 levels (Invitrogen, catalog no. BMS2043). Both ELISAs were run in a Thermo Labsystems Multiskan instrument, EX at 450 nm according to the manufacturer's instructions (RayBiotech & Thermo Fisher Scientific). For serum isolation from human blood (healthy donor and tumor patient blood), we collected the blood in a tube that contained no anticoagulant and allowed the blood to clot for 30 minutes at room temperature. Then we centrifuged at 1,000 × g for 10 minutes in a refrigerated centrifuge machine. The serum was separated from the clotted blood and analyzed for different immunoglobulins (IgG, IgM, IgA) using a nephelometer instrument (BN ProSpec System, Siemens Healthineers) and a system kit specific to BN ProSpec. The IgG subsets from cell culture (Tumor PBMC and Breg depleted tumor PBMC) supernatants were analyzed using the IgG subclass human ELISA kit (Thermo Fisher Scientific, catalog no. 99–

1000). Kit based standard IL10, IL21, and IgGs were used to develop a standard curve.

Ex vivo T-cell suppression assay

Magnetic bead–sorted CD19$^+$CD39$^-$ Breg cells (1×10^5 cells) from breast cancer patients' blood were cocultured with purified autologous naïve T cells (2×10^5 cells) activated with anti-CD3/anti-CD28 for 72 hours. From each culture experiment, flow cytometry was used to look for IFNγ, FOXP3 expression, and KI67, and annexin-V positivity in T cells. The change in percentage of IFNγ$^+$, FOXP3$^+$, KI67$^+$ and annexin-V$^+$ CD4$^+$ cells compared with CD4$^+$ cells that were cultured alone was calculated. Similarly, CD4$^+$ T-cell proliferation was monitored by the CFSE (BioLegend, catalog no. 423801) dilution assay. From a prepared 5-μmol/L working solution of CFSE, 100 μL of CFSE solution was dissolved in 900 μL of PBS containing 5×10^5 to 10×10^5 naïve T cells. This was incubated for 20 minutes at 37°C in the dark. Staining was quenched by adding 5 times the initial staining volume of 10% FBS cell culture media. The cells were then pelleted and resuspended in a cell culture pre-warmed media. After data acquisition on a flow cytometer (BD FACS Verse), the cell-proliferation index was calculated using FlowJo software.

Transcriptome analysis

RNA-array data containing three B-cell populations CD19$^+$CD24^{hi}CD38^{hi}, CD19$^+$CD24$^+$CD38$^-$, and CD19$^+$CD24^{int}CD38^{int} cells from 5 healthy donors with the identifier GSE76272 was downloaded from the Gene Expression Omnibus (GEO) database. The normalized gene expression data was downloaded in Excel format. A log2 fold change and a Student t test were carried out in Excel to identify the significant differentially expressed genes. At first, only significant genes were chosen using $P < 0.05$ as a cut-off value, followed by selecting the top 50 up- and downregulated genes. Surface-expressing genes were selected by using the Ingenuity Pathway Analysis (IPA) programme (QIAGEN; ref. 19). Heatmap analysis for transcriptomic data was performed using Multiple Experiment Viewer (MeV_4_8) software (20).

Semi-qPCR amplification of germline and AICDA (AID) transcripts and real-time PCR of BCL6

Semi-qPCR was conducted for the detection of isotype class-specific GLTs and AID. According to the manufacturer's protocols, RNA was isolated from the CD40LG+IL4+IL10—treated PBMCs (germline transcription detection, already mentioned Cell culture) cells using the TRIzol reagent (Thermo Fisher Scientific, catalog no. 15596026). cDNA synthesis was performed with 500 ng of RNA using the cDNA Synthesis Kit (Clontech TaKaRa, catalog no. RR037A). Amplification of 1,000 ng of the cDNA was conducted using specific primers and PCR cycles (Supplementary Table S6). The mean intensity of each band was evaluated using Image J (version 1.53k). Then, using Excel, the fold change was calculated. qPCR analysis of Bcl6 was performed using FastStart Essential DNA Green Master (Roche, catalog no. 06402712001) and run on a GeneAmpPCR 2720 (Applied Biosystems). RNA and cDNA synthesis for qPCR analysis was performed as described for PCR. The melting curve was used to assess amplification products using SYBR-green detection with the LC96 SW1.1 software. The data were analyzed using $2^{-\Delta\Delta Ct}$ method, with β-actin serving as housekeeping controls.

Mass spectroscopy

CD19$^+$B, CD19$^+$CD39$^-$ Breg and CD19$^+$CD39$^+$ non-Breg cell subsets were purified using magnetic beads as described in *Immune*

subset isolation. For adenosine detection, 10,000 cells from each group were cultured in 200 μL PBS in 96-well plates for 40 minutes in the presence of 20 μmol/L ATP (Himedia, catalog no. TC085–5G). One B-cell sample was also treated with a CD73 inhibitor [Adenosine 5′-(α,β-methylene)diphosphate; Sigma-Aldrich, catalog no. M3763] at a concentration of 50 μmol/L. Cell supernatants were collected, centrifuged at $6,000 \times g$ for 2 minutes, boiled for 2 minutes to inactivate ADO-degrading enzymes, and kept at $-80°C$ for further investigation. Adenosine levels were determined using an electrospray-mass spectrometry (ESI–MS) direct infusion (Waters Xevo G2-S QTof) by measuring the intensity of the Adenosine Mass (268). For tuning and calibration for ESI, MS-QTof (Machine name: Water xevo g2 xs-QTof), leucine enkephalin (molar mass 555.62 g/mol) was used. The detection mode was +ve ion mode and the collision energy was 6. The source capillary (kV) was 3.00, the sampling concentration was 40 and the source offset was 80. The temperature of the source was $100°C$ and desolvation was $250°C$. The concentration of the gas (L/h) for gas flow was 50 L/h and the desolvation of gas (L/h) was 400 L/h. The sample injection volume was 5 μL, and the acquisition running time was a minute. The data was analyzed by Masslynx-v.4.1 software.

Cytokine bead array

Using an anti-human Th1/Th2/Th17 CBA array kit (BD Biosciences, catalog no. 560484) according to the manufacturer's instructions, the concentrations of IL2, IL4, IL6, IL10, IL17, TNFα, and IFNγ in healthy donor and tumor patient–derived serum, as well as tumor patient–derived non-Breg and Breg cell–derived cultured supernatant, were evaluated simultaneously. The serum isolation procedure was as described above (see *ELISA assay*). The BD FACS Verse machine was used to gather the data, and FCAP Array Software v3.0 from BD Biosciences was used to analyze it.

Statistical analysis

Data analysis was performed using GraphPad Prism 7.0 software. All data was performed in triplicate. ±SDM is calculated using GraphPad Prism 7.0 software. The unpaired and paired Student t tests, ANOVA and χ^2 tests were used to evaluate the significance of differences observed between groups, accepting the value of $P < 0.05$ as statistically significant.

Data availability statement

The microarray data analyzed in this study were obtained from GEO at GSE76272. Other data generated in this study are available within the article and its Supplementary Data files or from the corresponding author upon reasonable request.

Results

Breg cells can be found in human breast cancers

Tumor-infiltrating lymphocytes are important modulators of tumor progression (21, 22). While T cells have been extensively studied, the role of B cells in regulating antitumor immunity is less well understood (23). Such a limited understanding of B cells' role in tumor immunology prompted us to explore the atlas of B-cell subsets in the breast tumor microenvironment.

We investigated B-cell subset marker expression, cytokine production, and antibody response in patients with breast cancer and compared them with age and gender-matched healthy people (Supplementary Fig. S1A). On the basis of our concatenated flow-cytometry data (**Fig. 1A**) of lymphocytes obtained from healthy individuals and breast cancer patients' blood, we found a higher percentage of B cells in blood from patients with cancer. As B cells are primarily responsible for antibody production, we analyzed serum levels of immunoglobulins, observing that the level of serum-IgG was significantly lower and the level of IgM was significantly higher in cancer patients' serum than in serum from healthy controls, while the level of IgA remained unchanged (**Fig. 1B**).

We next conducted a thorough investigation of B-cell subsets and their roles in breast cancer dynamics using multiparametric flow cytometry. A detailed t-SNE analysis of $CD19^+$-gated B cells (**Fig. 1C**) enabled the identification and differential expression of four B-cell subpopulations in the peripheral blood of patients with breast cancer: plasma B cells/plasmablasts ($CD19^+CD38^{hi}CD27^{hi}$), mature B cells ($CD19^+CD24^{int}CD38^{int}$), memory B cells ($CD19^+CD24^{hi}CD27^+$), and transitional B cells ($CD19^+CD24^{hi}CD38^{hi}$).

The number of transitional B cells was significantly greater in cancer patients' blood than in blood from healthy donors, while the percentage of $CD27^+$ memory B cells and their eventual $CD27^{hi}CD38^{hi}$ plasma B cells was lower (**Fig. 1C**). This finding was validated in a cohort of 10 healthy females and 15 patients with breast cancer (**Fig. 1D**). Apart from the predicted classical Th2-cytokine bias response (IFNγ skewed to IL4), cytometric bead array results revealed a significantly higher level of IL10 in breast cancer patients' serum (**Fig. 1E**; Supplementary Fig. S1B).

We investigated the intracellular level of IL10 in the tumor-associated transitional B-cell subset because of the high frequency of transitional B cells in the peripheral blood, increased IL10 level in the serum of patients with breast cancer, and previously reported IL10-positivity as a widely used marker for Breg cells identification (24). From the tumor patient's blood, intracellular IL10 labelling revealed that a considerably larger percentage of $CD19^+CD24^{hi}CD38^{hi}$ transitional B cells were $IL10^+$ than mature or memory B cells (**Figs. 1F**; Supplementary Fig. S1C). Aside from IL10, transitional B cells secrete significantly less IFNγ, IL6, and IL17 than the other B-cell subsets (**Figs. 1G**; Supplementary Fig. S1D). All of this evidence confirmed that transitional $CD19^+CD24^{hi}CD38^{hi}$ B cells were more prevalent in patients with cancer and contributed to a high amount of IL10 secretion. In the tumor microenvironment, these IL10-producing transitional B cells are Breg cells.

$CD19^+CD24^{hi}CD38^{hi}$ Breg cells increase with breast tumor stage

The fact that we found that patients with breast cancer have a higher frequency of IL10-secreting transitional Breg cells encouraged us to investigate the expression pattern of $IL10^+$ Breg cells with tumor advancement. Therefore, we used flow cytometry to investigate the frequency distribution of these cells in various pathophysiological conditions. **Figure 2A** shows that the percentage of $CD19^+CD24^{hi}CD38^{hi}$ Breg cells in the peripheral circulation (10%–12%) and tissues (22%) of the patients with breast cancer were higher than in healthy donor PBMCs. Blood from patients with pathologic disorders such as autoimmune inflammatory disease (RA), on the other hand, showed lower levels of Breg cells than healthy individuals. Breg-cell percentage has also been reported to be low in autoimmune disorders (25). We also checked the percentage of $CD19^+CD24^{hi}CD38^{hi}$ Breg cells in HBV-infected patients' blood and found that they had a similar expression level as healthy individuals. In Graves' disease and systemic lupus erythematosus patients, $CD19^+CD24^{hi}CD27^+$ B cells have been defined as Breg cells (11, 26). So, we investigated their status and observed that the frequency of this cell type was lower in breast cancer patients' blood than in healthy donor's blood (Supplementary Fig. S2A),
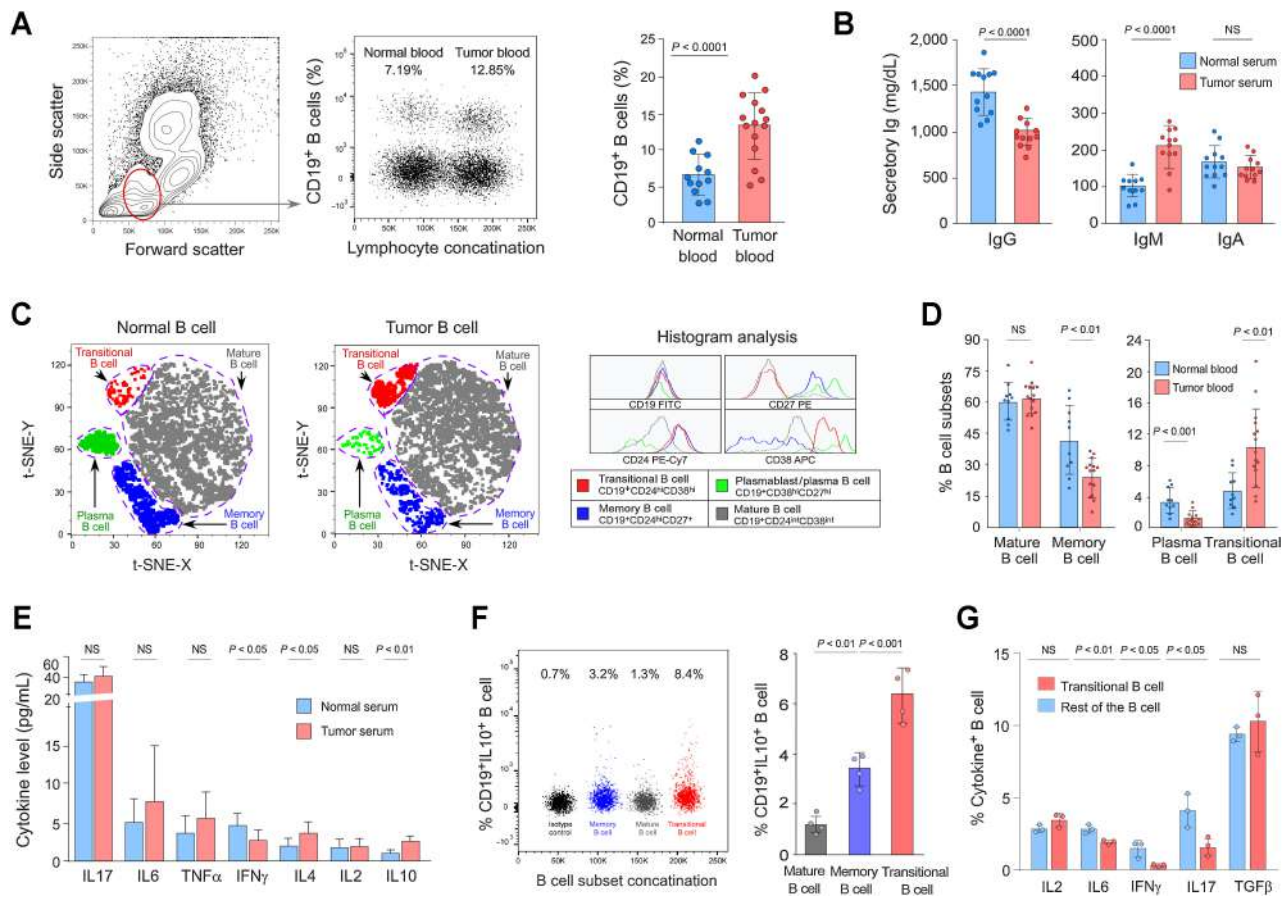
Figure 1.
Prevalence of IL10-producing transitional B cells in breast tumor milieu. **A,** A representative flow-cytometry concatenated plot and corresponding bar graph shows the percentage of CD19$^+$ B cells in lymphocytes from the peripheral circulation of patients with breast cancer ($n = 15$) and healthy individuals ($n = 12$). **B,** The bar graph shows the levels of serum IgG, IgM, and IgA amongst the same patients with breast cancer and healthy individuals analyzed in (**A**). **C,** The t-SNE cluster displays the distribution of four major B-cell subsets within the CD19$^+$ B-cell compartment and compares the difference in frequency of these cell clusters amongst patients with breast cancer and healthy individual's blood. The major B-cell subsets are transitional B cells (red), plasma B cells (green), memory B cells (blue), and mature B cells (grey). Histogram plots show the comparison between surface marker (CD19, CD24, CD38, and CD27) expression in CD19$^+$ B-cell populations in the gated regions. **D,** Cumulative results of the percentage of mature, memory, plasma, and transitional B cells within the CD19$^+$ B-cell populations in blood from patients with breast cancer ($n = 15$) and healthy individuals ($n = 10$), are represented in the bar graph. Each dot represents data generated from an individual. **E,** Simultaneous assessment of serum IL2, IL4, IL6, IL10, IL17, IFNγ, and TNFα levels was performed by anti-human CBA array kit using serum from patients with breast cancer ($n = 22$) and healthy individuals ($n = 14$). Each point represents data generated from individual (healthy donor/tumor patient) serum. **F,** Representative flow-cytometric concatenated dot plot depicting IL10 expression in different B-cell subsets gated from total B cells in PBMCs from patients with breast cancer: transitional (red), mature (grey), memory (blue) B cells, and Isotype control (Black). The cumulative results from multiple samples ($n = 4$) are represented in a bar graph. The bar chart represents ±SDM of percent IL10$^+$ B cells within different B-cell compartments as shown in 4 sets of independent experiments. **G,** The bar graph depicts the cumulative flow cytometric results of expression of several cytokines by transitional B cells and the rest of the B cells in PBMCs from patients with breast cancer ($n = 3$). Student t test was used for all statistical analysis in Fig. 1 and all the error bars are represented as mean ±SD.

Q10

implying that CD19$^+$CD24^{hi}CD38^{hi} transitional B cells are the only subset that increased in breast tumors.

The interaction between tumor and IL10-producing Breg cells was investigated further using flow cytometry. When comparing cancer patients' blood and tumor tissue with blood from their healthy counterparts, the percentage of IL10$^+$ B cells increased, indicating a positive association between Breg cells and tumors (**Fig. 2B**). We also used confocal microscopy to validate our findings (**Fig. 2C**). Supplementary Figure S2B depicts all the controls. After identifying an accumulation of Breg cells in breast tumors, we assessed the percentage of CD19$^+$CD24^{hi}CD38^{hi} Breg cells in the blood of patients with different stages of disease. Flow cytometry was used to determine the

percentage of Breg cells in the patient's blood (Supplementary Fig. S2C), and the multiple data points were then represented in a bar graph (**Fig. 2D**) revealing that the percentage of Breg was increased as the tumor stage advanced. Our findings collectively imply that CD19$^+$CD24^{hi}CD38^{hi} Breg cells increased in number during tumor development.

CD39-negativity is a signature marker for tumor-associated Breg cells

Intracellular IL10-positivity is the hallmark of Breg-cell identification (27). Being an intracellular protein, IL10 can be a signature molecule for Breg-cell identification but cannot be an isolation marker.
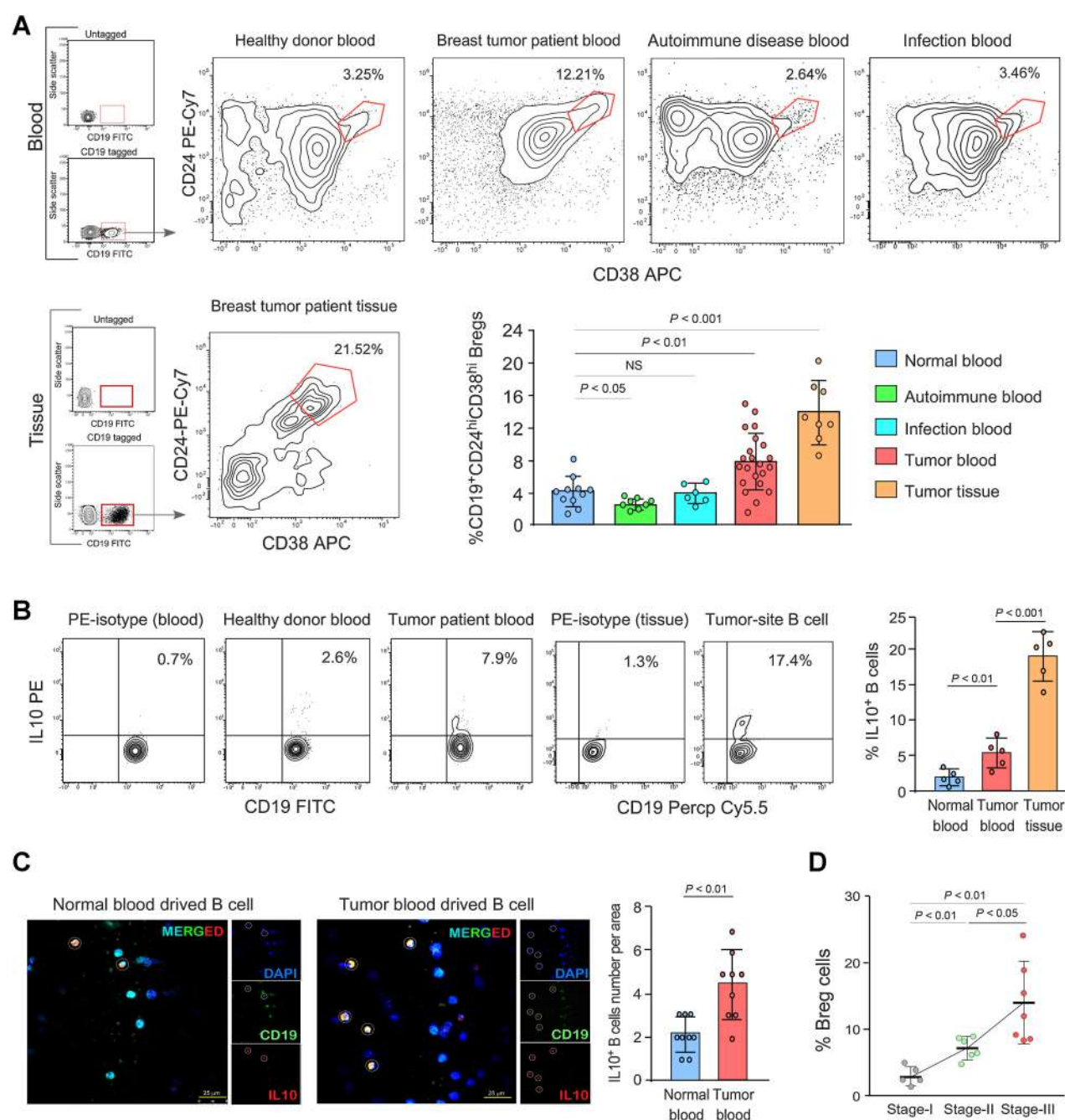
Figure 2.
Phenotypic characterization of the IL10-producing Breg cells. **A,** Flow-cytometric representation of CD19$^+$CD24^{hi}CD38^{hi} Breg-cell populations in the blood of healthy donors, patients with breast cancer, patients with RA, HBV-infected patients, and tumor-infiltrating lymphocytes. The scatter plot shows the frequencies of CD19$^+$CD24^{hi}CD38^{hi} Breg cells in breast cancer patients' blood ($n = 22$), healthy individuals ($n = 11$), patients with RA ($n = 8$), HBV-infected patients ($n = 6$) and in tumor-infiltrating lymphocytes ($n = 8$). **B,** Representative flow-cytometry data showing the percentage of CD19$^+$IL10$^+$ B cells in healthy people ($n = 5$), breast cancer patients' blood ($n = 5$), and tumor tissue ($n = 5$). The cumulative results from multiple samples are represented in a bar graph. Values are mean $\pm$ SD or representatives of 5 sets of independent data points. **C,** Confocal images showing the expression of IL10 in CD19$^+$ B cells in the peripheral circulation of patients with breast cancer compared with healthy individuals. The cells were examined under a Leica confocal microscope at 63× magnification. A representative bar graph depicts the number of IL10$^+$ B cells per area taken from normal and tumor blood–derived B cell. Three images were captured from each set of experiments ($n = 3$), for a total of nine points on the graph. **D,** A representative graph demonstrating the positive correlation between the percentage of Breg cells (isolated from peripheral circulation of tumor patient) and tumor progression. The number of patients analyzed in stage I is 5, stage II is 6, and stage III is 7. Student t test was used for all statistical analysis in Fig. 2 and all the error bars are represented as mean $\pm$ SD.
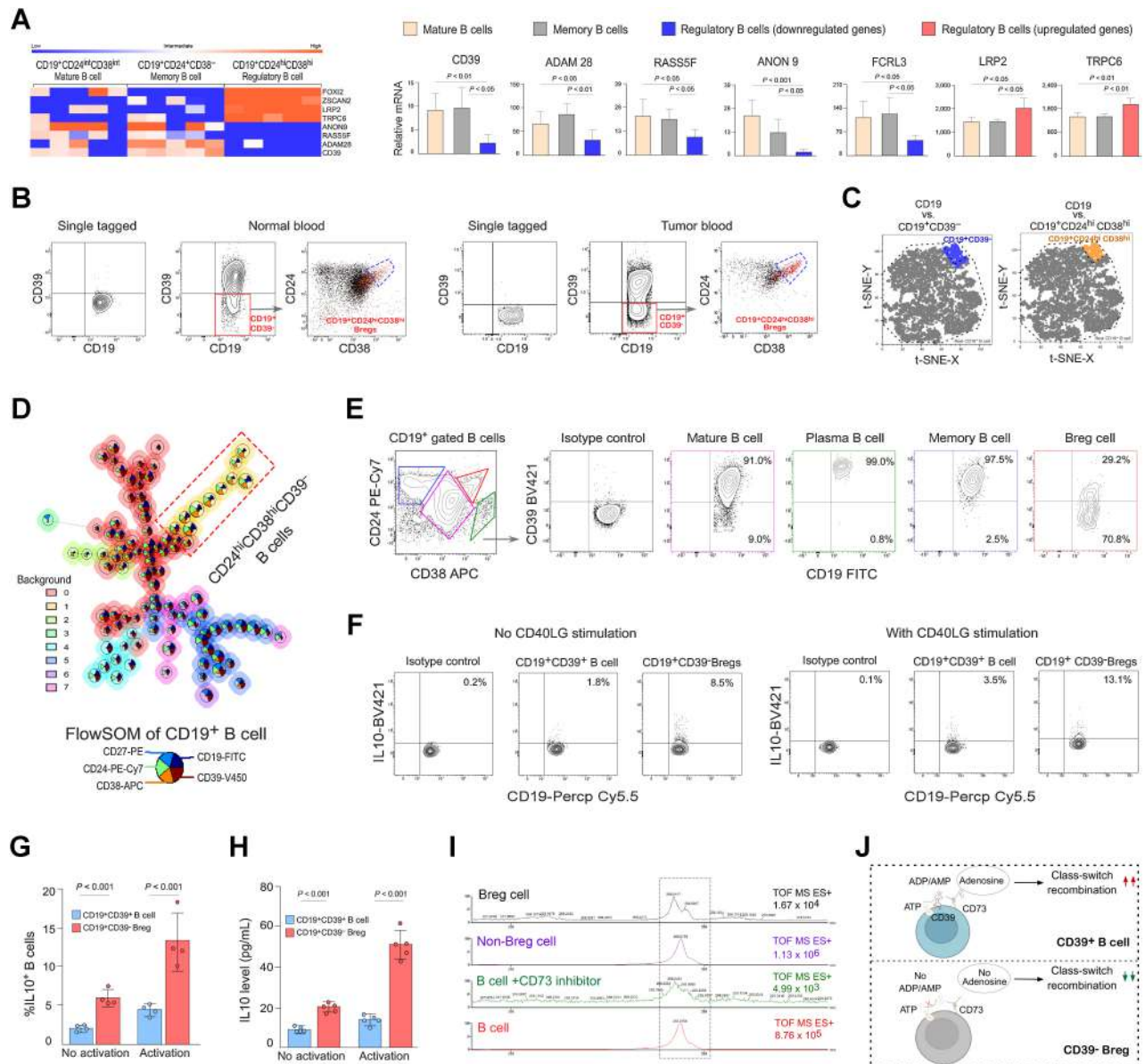
Figure 3.
CD39-negativity is a signature marker for tumor-associated IL10-producing Breg cells. **A,** In silico analysis of transcriptome data from CD19+CD24hiCD38hi (regulatory), CD19+CD24intCD38int (mature), and CD19+CD24+CD38− (memory) B cells sorted from the PBMCs of 5 healthy donors. The data were obtained from the GEO database (GSE76272). Heatmap analysis depicts some of the up- and downregulated genes (surface and transcription factors) in the three subsets of cells (left). The right panels demonstrate only top surface-expressing genes (upregulated and downregulated) in the Breg-cell compartment. *CD39* (*ENTPD1*) was found to be one of the top downregulated surface marker genes in the Breg-cell (CD19+CD24hiCD38hi) compartment compared with the other two B-cell subsets. **B,** Flow-cytometric representation of CD39-negativity in total CD19+ B-cell populations and status of CD24 and CD38 in CD39− negative populations in the peripheral circulation of a healthy donor and a patient with breast cancer. **C,** The representative t-SNE plot depicts the amount as well as the position of CD19+CD39− (blue) and CD19+CD24hiCD38hi (orange) cells within total CD19+ (grey) B cells (PBMCs). **D,** Representative FlowSOM analysis depicting seven different B-cell populations in cancer patient's blood. Clusters are represented as circles with star plots illustrating cluster median marker intensities. Meta-clustering is represented by the background color. The identified yellow branch depicts CD19+CD24hiCD38hiCD39− Breg cells. **E,** Representative flow-cytometry data show CD39 expression in various tumor patients PBMC-derived B-cell subsets. **F,** Flow-cytometry plot of IL10 positivity in CD19+CD39− and CD19+CD39+ B cells (isolated from tumor PBMCs) with or without CD40LG (CD154) activation. **G,** Bar graph demonstrated the flow-cytometric cumulative results of IL10 positivity in CD19+CD39− and CD19+CD39+ B cells (*n* = 4). **H,** Supernatants from purified B-cell subsets from PBMCs of tumor patient (*n* = 5) with or without CD40LG (CD154) activation were tested for the presence of IL10 by ELISA. The data are shown as mean ± SD. **I,** Mass spectrometry analysis of adenosine generation in the supernatants of magnetic sorted CD19+ B cells from tumor patient's blood (represented as red color), CD19+ B cells in presence of CD73 inhibitor (represented as green color), CD19+CD39+ non-Breg (represented as violet color), and CD19+CD39− Breg cells (represented as black color) after addition of exogenous ATP. **J,** Comparative analysis of adenosine secretion between CD39− and CD39+ B cells that are involved in CSR, represented schematically. Student *t* test was used for all statistical analysis in Fig. 3 and all the error bars are represented as mean ± SD.

However, because they have three highly expressed cell surface markers, identified IL10-producing CD19$^+$CD24^{hi}CD38^{hi} Breg cells have limitations in purifying functional B cells. These are the major reasons behind many functional aspects of the Breg cells being still ill-defined.

We performed a transcriptome analysis using data from a GEO database (GSE76272) to identify distinct Breg-cell surface characteristic markers (10). At first, we shortlisted only significant ($P < 0.05$) top 50 upregulated and downregulated genes in CD24^{hi}CD38^{hi} Breg cells and compared them with CD24^{int}CD38^{int} mature and CD24$^+$CD38$^-$ memory B-cell subsets (**Fig. 3A**, left). From the IPA, only surface-expressing genes were evaluated (**Fig. 3A**, right). CD39 (ENTPD1), an ATP-hydrolase that converts ATP to ADP/AMP, is one of the most promising surface markers, with minimal surface expression in CD19$^+$CD24^{hi}CD38^{hi} Breg cells and high expression in both mature and memory B-cell subsets. Sean C. Bendall's group also noticed a similar pattern of CD39 expression in their single-cell multi-omics analysis (28).

Our multicolor flow-cytometric dot-contour overlay analysis from the PBMC of healthy individuals and tumor patients (**Fig. 3B**) confirmed that CD39$^-$ B cells are CD24^{hi}CD38^{hi}. CD19$^+$CD39$^-$ cells, highlighted as red (red box), and the rest of the grey dots are CD19$^+$CD39$^+$. In the same CD38 versus CD24 plot, we overlaid this compartment of cells. The vast majority of CD19$^+$CD39$^-$ cells (red) were CD19$^+$CD24^{hi}CD38^{hi}. This finding was confirmed in a cohort of breast cancer patients' samples, where there was no discernible difference in the frequency of CD19$^+$CD39$^-$, CD19$^+$CD24^{hi}CD38^{hi}, and CD19$^+$CD24^{hi}CD38^{hi}CD39$^-$ B cells (Supplementary Fig. S3A). Clustering (t-SNE) and visualization (FlowSOM) plugins were used to analyze the high-dimensional flow-cytometric data. Within the entire breast cancer patients' B-cell pool, CD39$^-$ B cells were limited in the same place as CD24^{hi}CD38^{hi} cells, and their numbers were nearly comparable (**Fig. 3C**; Supplementary Fig. S3B). The FlowSOM analysis revealed a B-cell subset with negligible CD39 expression but high CD24 and CD38 expression (**Fig. 3D**).

It is worth noting in this context that previously reported CD19$^+$CD39$^+$ B cells are immunosuppressive in nature (26, 29). But these cells are not altered in tumor condition. Only CD19$^+$CD39$^-$ B cells, which are also CD19$^+$CD24^{hi}CD38^{hi} are increased in tumor conditions (Supplementary Fig. S3C and S3D). We examined numerous features of the CD19$^+$CD39$^-$ Breg-cell subset to better characterize it. We checked various B-cell developmental markers, including PD-L1, IgM, IgD, and CD73 (Supplementary Figs. S3E and S3F) and found that CD39-positivity was strongly associated with three of the B-cell subsets in breast cancers, including mature and, most notably, memory B cells and plasma B cells, whereas CD39$^-$ B cells were not associated with any of the aforementioned subsets except for transitional B cells (**Fig. 3E**; Supplementary Fig. S3G).

CD19$^+$CD39$^-$ was found to be an alternate Breg-cell isolation marker to CD24^{hi}CD38^{hi} based on transcriptome and flow-cytometric data. We evaluated IL10 status to ensure that CD19$^+$CD39$^-$ cells were Breg cells. We used a customized magnetic bead–sorting method to separate CD19$^+$CD39$^+$ and CD19$^+$CD39$^-$ B cells from breast cancer patients' blood and activated them for 72 hours in the presence of CD40LG. CD39$^-$ B cells made up a higher percentage and secreted more IL10 than CD39$^+$ B cells, according to intracellular labelling from flow cytometry (**Fig. 3F** and **G**) and cultural supernatants data from ELISA (**Fig. 3H**). When CD40LG (CD40's counterpart) was involved, IL10 was elevated in the CD19$^+$CD39$^-$ Breg-cell compartment. Apart from IL10, our cytometric bead array data from the cell supernatant of CD19$^+$CD39$^+$ non-Breg and CD19$^+$CD39$^-$ Breg cells cultured for 72 hours in the presence of CD40LG revealed that CD39$^-$ B cells

produced significantly lower levels of pro-inflammatory cytokines like IL6, IFNγ, and IL17 than CD39$^+$ B cells (Supplementary Fig. S3H). When isolated total B cells and Breg cells were activated and cultured in the presence of LPS, the CD39$^-$ Breg percentage was maintained in both cultures even after 7 days (Supplementary Fig. S4A). We also found that Breg cells never re-differentiated from mature B cells in post-Breg depleted samples (Supplementary Fig. S4B) under exogenous stimulus. (CD40LG with IL2 and IL10). These data indicate that the CD39$^-$ Breg-cell population is a stable, self-contained population and does not re-differentiate.

We also tested the class-switching properties of Breg cells and observed that the CD39$^-$ B-cell subset was class-switch impaired because it could not synthesize adenosine (**Fig. 3I** and **J**; Supplementary Fig. S4C) and exogenous adenosine can salvage tumor derived B cells CSR ability (Supplementary Fig. S4D). This class-switch deficient feature of CD39$^-$ Breg cells makes it a different B-cell subset from other conventional B-cell subsets.

Tumor-associated Breg cells have immunoregulatory functions

The identification of suitable surface markers for Breg cells, as well as their prevalence in the breast tumor microenvironment, prompted us to investigate the functional attributes of these CD19$^+$CD39$^-$ Breg cells. To assess their immunoregulatory function, we isolated CD19$^+$CD39$^-$ cells from PBMCs from patients with breast cancer (Supplementary Fig. S5A) and cocultured them for 72 hours with purified autologous naïve CD4$^+$ T cells (Supplementary Fig. S5B and S5C). The coculture experiment is depicted schematically in Supplementary Fig. S5D. Anti-CD3 and anti-CD28 were used to stimulate naïve CD4$^+$ T cells, and the frequencies of CD4$^+$IFNγ^+, CD4$^+$FOXP3$^+$, and CD4$^+$Ki67$^+$ cells were assessed using flow cytometry.

When CD4$^+$ T cells were cocultured with CD19$^+$CD39$^-$ Breg cells, it was observed that Breg cells had an inhibitory effect on IFNγ production (**Fig. 4A**). The inhibitory effect was proportional to the cell ratio (Supplementary Fig. S5E). The Ki67-positivity assay demonstrated that CD19$^+$CD39$^-$ Breg cells suppressed the proliferation of activated CD4$^+$ T cells (**Fig. 4B**). The Breg cells also induced effector T cell death when they were cultured together (Supplementary Fig. S5F). In addition, the immunosuppressive CD19$^+$CD39$^-$ Breg-cell subset promoted the generation of suppressive CD4$^+$FOXP3$^+$ Treg cells from cocultured autologous activated T cells (**Fig. 4C**). Finally, coculture with Breg cells resulted in reduced cell proliferation of activated CD4$^+$ T cells, as measured by the proliferation index level (CFSE dilution; **Fig. 4D**). All of this evidence suggests the CD19$^+$CD39$^-$ Breg cells generated in the tumor being immunosuppressive and maintaining immunogenic tolerance in patients with breast cancer.

CD39$^-$ Breg cells deregulate CSR

The adaptive immune response is characterized by somatic DNA recombination such as the CSR required to alter the antibody's effector function. H-chain class switching occurs in three stages: germline gene transcription (GLT), DNA recombination, and B-cell differentiation into memory B cells, followed by Ig-secreting plasma cells (**Fig. 5A**; ref. 30). **Figure 1** shows that Breg-cell frequency was negatively related to memory and plasma B cells. In blood from a cohort of 10 healthy individuals and 10 patients with breast cancer, we detected that the frequency of Breg cells versus memory B cells and plasma B cells has an inverse correlation in patients with breast cancer (Supplementary Fig. S6A). From this observation, we hypothesized that Breg cells may
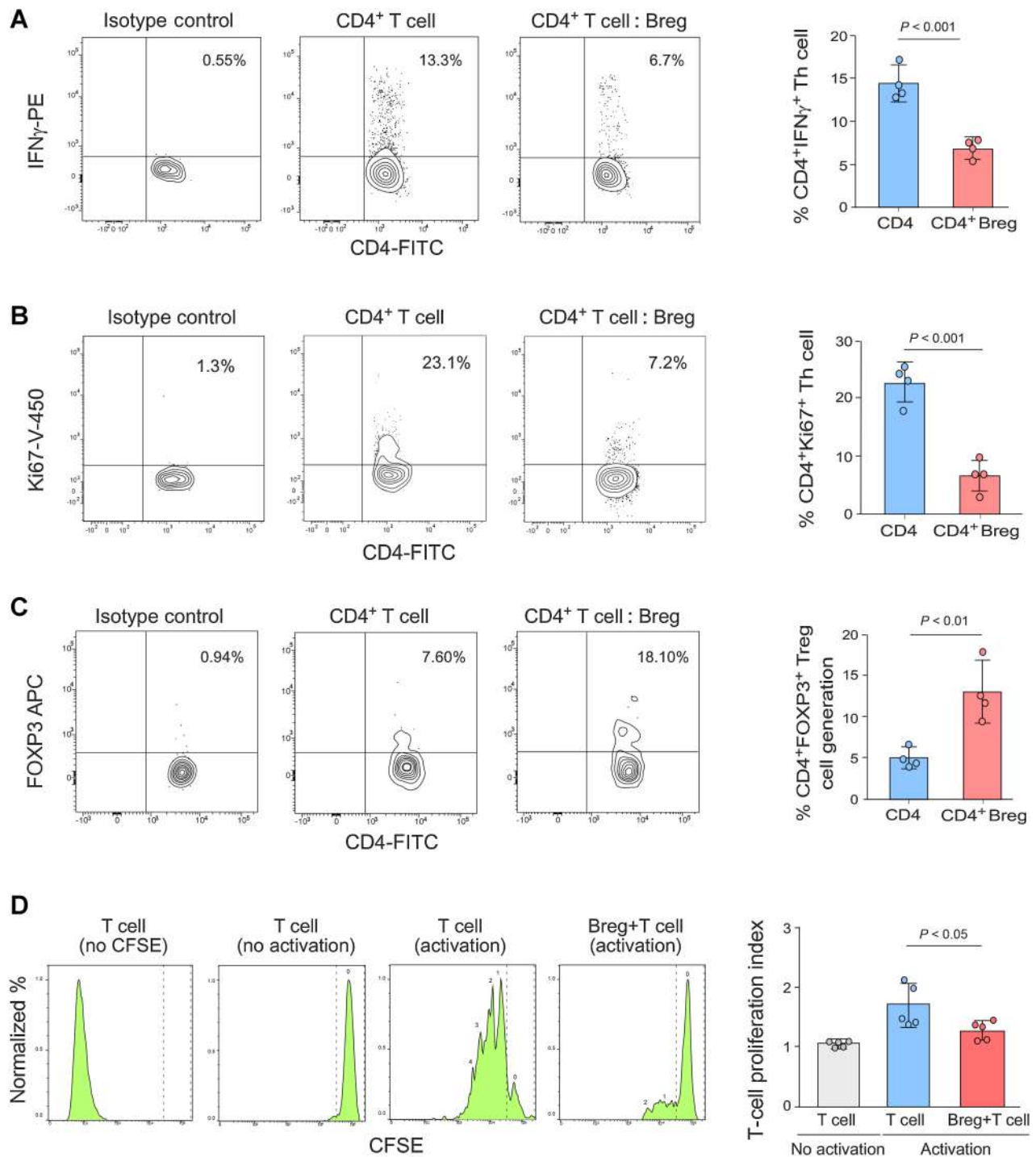
Figure 4.
Suppressive function of tumor-associated CD19$^+$CD39$^-$ Breg cells. **A,** Representative flow-cytometry plot depicting the suppression of CD4$^+$IFNγ^+ Th1 cells when *ex vivo* cocultured with CD19$^+$CD39$^-$ Breg cells (isolated from tumor PBMC, $n = 4$). **B,** Flow-cytometry analysis of the inhibitory effects of Breg cells (isolated from tumor PBMC, $n = 4$) on CD4$^+$ T-cell proliferation (Ki67-positivity). **C,** The percentage of CD4$^+$FOXP3$^+$ Treg cells generated from CD4$^+$ T cells when cocultured *ex vivo* with CD19$^+$CD39$^-$ Breg cells (isolated from tumor PBMC, $n = 4$). **D,** CD4$^+$ responder T-cell proliferation (stimulated with anti-CD3/anti-CD28) was measured by a CFSE-dilution assay in the presence of CD19$^+$CD39$^-$ Breg cells (isolated from tumor PBMC, $n = 5$). Cumulative results of the responder T cells' proliferation index from independent experiments are represented in the bar diagram. Cumulative results of the CD4$^+$IFNγ^+, CD4$^+$FOXP3$^+$, and CD4$^+$Ki67$^+$ percentage with or without the presence of Breg cells are represented in the bar graph. Each dot represents data generated from each of 4 independent experiments with cells from different patients with breast cancer. Student *t* test was used for all statistical analysis in Fig. 4 and all the error bars are represented as mean ± SD.

Figure 5.
CD19$^+$CD39$^-$ Breg cells hinder B-cell differentiation by limiting germline transcription involved in CSR for antibody production in patients with breast cancer. **A,** A diagram of the stages of B-cell development, from B-cell activation to the formation of plasma cells that make antibodies. **B,** Flow-cytometric representation of the memory B-cell subtype based on CD19, CD27, and IgD expression from tumor patient blood. Three B-cell subpopulations are defined by the expression of IgD and CD27 within CD19$^+$ B cells: Naïve (IgD$^+$CD27$^-$), Unswitched memory (IgD$^+$CD27$^+$), and switched memory (IgD$^-$CD27$^+$). The expression of surface IgG and IgM in these B cells is represented in a concatenated format. **C,** Schematic depiction of experiments for memory/plasma/CSR. **D,** Representative flow-cytometric plot depicting the *ex vivo* differentiation of class-switched memory B cells. Results from multiple different experiments are represented as ± SDM ($n = 4$). **E,** Representative flow-cytometric plot depicting the *ex vivo* differentiation of antibody-producing plasma B cells. Results from multiple different experiments are represented as ± SDM ($n = 4$). **F,** Representative DNA-gel electrophoresis of PCR product demonstrating the effect of Breg cells on the expression of germline-γ1, -γ2, and *AID* transcripts. **G,** The cumulative results from multiple samples obtained from PCR (analyzed in ImageJ) are represented in a bar graph. Values are mean ± SD representatives of 3 sets of independent experiments generated from different breast cancer samples. **H,** Representative flow-cytometric plot depicting the *ex vivo* differentiation of the *ex vivo* development of IgG-producing B cells in cultured whole PBMCs and Breg-depleted PBMCs from patients with breast cancer. Results from multiple different experiments are represented as ± SDM ($n = 4$). **I,** Supernatants from cultured whole PBMCs and Breg-cell depleted PBMCs from patients with breast cancer ($n = 4$) were tested for the presence of secretory IgG1 and IgG2 by ELISA. Student *t* test was used for all statistical analysis in Fig. 5 and all the error bars are represented as mean ± SD.

be interfering with the establishment of memory B cells. Memory B cells are classified into two groups based on their IgG and IgM status. Non–class-switched memory B cells (CD19$^+$CD27$^+$IgD$^+$) do not undergo class-switching and generate IgM, whereas class-switched memory B cells (CD19$^+$CD27$^+$IgD$^-$) undergo CSR to produce IgG (**Fig. 5B**; Supplementary Fig. S6B) (31).

We depleted Breg cells from breast cancer patients' PBMC and cultured them *ex vivo* for 7 days in media containing either CD40LG+IL2+IL4 to generate memory phenotype B cells, CD40LG+IL2+IL10 to generate plasma cells, or CD40LG+IL4+IL10 to promote germline-γ1/-γ2 and AID transcription to answer the enigma of Breg cells' impact on germline gene transcription (GLT), and B-cell differentiation (**Fig. 5C**). Flow cytometry was used to analyze the differentiation of memory B cells (CD19$^+$CD27$^+$), more precisely, class-switched (CD19$^+$CD27$^+$IgD$^-$)/non–class-switched (CD19$^+$CD27$^+$IgD$^+$) memory B cells, and plasma B cells (CD38^{hi}CD138$^+$), and PCR was used to analyze CSR of germline-γ1/-γ2 and AID. Our flow-cytometry analysis demonstrated a rise in memory B cell percentages, specifically class-switched memory (**Fig. 5D**). and plasma B cells (**Fig. 5E**) in Breg-depleted conditions The class-switched transcripts germline-γ1/-γ2 and *AID* were also amplified in such conditions (**Fig. 5F** and **G**). In this regard, we investigated the role of mature B cells in raising AID levels in Breg-depleted samples. We demonstrated that while a small increase in the fraction of mature B cells could contribute to an increase in AID expression under Breg-depleted conditions, it could not be the sole cause of a large change in AID expression (Supplementary Fig. S6C). In the Breg-depleted condition, the elevated AID level eventually leads to greater surface level IgG (**Fig. 5H**) and secreted antibodies (IgG1 and IgG2; **Fig. 5I**) from B cells.

CD39$^-$ Breg cells disrupt memory to plasma B-cell differentiation

Next, we generated plasma cells *ex vivo* by incubating Breg-depleted patients' PBMC with plasma B cell–specific stimuli in combination with CD40LG+IL2+IL10 (**Fig. 6A**) to investigate the role of Breg cells in the differentiation of Ig-secreting plasma B cells. When Breg cells were eliminated from the cancer patient lymphocyte pool, the frequency of CD38^{hi}CD138$^+$ plasma B cells increased significantly (from 2% to 45%; **Fig. 6B**, top; **Fig. 6C**), as did the frequency of class-switched memory B cells (from 7% to 37%; **Fig. 6B**, bottom; **Fig. 6C**) after 14 days of culture. We also observed that Breg-depletion alone could cause memory B-cell generation even in the absence of any memory B cell–specific activation (**Fig. 6A–C**). Our UMAP plots also demonstrate that memory and plasma B-cell cluster frequencies increased in the Breg-depleted condition (**Fig. 6D**).

All of this evidence supports the notion that CD19$^+$CD39$^-$ Breg cells have a negative impact on CSR, particularly at the level of GLTs and AID expression. As a result, the generation of class-switched memory B cells is halted, and the number of antibody-producing plasma B cells is reduced resulting in a lower IgG level, which provides an explanation as to why we detected less IgG in breast cancer patients' serum (**Fig. 1B**).

Breg cells inhibit antibody production by regulating Tfh-cell responses

Previous investigations on B-cell biology have demonstrated that Tfh cells are one of the important immune subsets that trigger class-switching by producing IL21 (**Fig. 5A**; ref. 32). As our data

from **Figs. 5** and **6** indicate that Breg cells prevent CSR, we investigated whether Breg cells could disrupt CSR by modulating Tfh-cell responses. To do this, purified naïve T cells (Supplementary Fig. S5B) were cocultured alone or with Breg cells (Supplementary Fig. S5A) and total conventional B cells except Breg (additional control) under Tfh cell–polarizing conditions.

During the process of Tfh-cell differentiation, we noticed that Breg cells had a considerable suppressive effect on CXCR5$^+$ programmed cell death protein 1 (PD-1)^{hi} Tfh-cell development (**Fig. 7A**), as well as the synthesis of the transcription factor BCL6 (**Fig. 7B**). Tfh-cell generation was unaffected by the addition of conventional B cells to the naïve T-cell culture. These data altogether suggest that downregulation of Tfh-cell responses were only halted in the presence of Breg cells. Tfh cells are a key source of IL21 (Supplementary Fig. S7A; ref. 33), and we found the percentage of CD4$^+$IL21$^+$ T cells was considerably lowered in the presence of Breg cells (**Fig. 7C**; Supplementary Fig. S7B). Following that, we looked at whether, apart from Tfh-cell differentiation and IL21 production, Breg cells had any negative impacts on IL21 levels from already generated Tfh cell. As a result, we ran another flow-cytometry experiment with the same number of Tfh cells from Breg culture, total B-cell culture (except Breg) or grown alone. This time, we observed that Breg cells could also inhibit IL21 production by already differentiated Tfh cells (**Fig. 7D**).

Next, we attempted to assess plasma-cell generation in relation to the Tfh cell–polarizing conditions. We designed an experiment in which we grew ongoing Tfh differentiated cells alone or with Breg cells and conventional B cells without Breg for 72 hours and collected cell supernatant, followed by a further 5 days of culture with autologous unstimulated B cells (excluding Breg) (**Fig. 7E**) to assess plasma B-cell generation.

Because recombinant IL21 was added as part of the Tfh-cell differentiation protocol, it was not clear whether the plasma-cell generation was mediated by exogenous IL21 or Tfh-cell secreted IL21. To answer this question, we performed a time-dependent ELISA of IL21 in the conditioned media and noticed that after 24 hours, the majority of the exogenously added IL21 bound to naïve T cells (Tfh cell–polarizing conditions). After 48 hours, the level of IL21 gradually increased in the culture supernatant and peaked at 72 hours (**Fig. 7F**). Although some background IL21 (recombinant IL21) existed in the cell supernatant after 72 hours, this basal IL21 level was the same for all culture conditions (T-cell alone, with Breg cells, and with B cells).

From the supernatants collected after 72 hours of Tfh-cell generation in various culture conditions, we observed that Breg cells suppressed the IL21 release from differentiating Tfh cells (**Fig. 7G**). As IL21 getting lowered after Breg engagement, a significant reduction in plasma B-cell generation was observed (**Fig. 7H**). All of these results suggested that Breg cells inhibit antibody responses by suppressing Tfh-cell differentiation and Tfh-cell IL21 production (Supplementary Fig. S7C).

Discussion

Antibody responses generated by B cells have the potential to destroy tumor cells, and IgG plays an important role in this process (34, 35). Numerous B-cell biology investigations have found that IgG levels in patients with metastatic breast cancer are much lower and IgM levels are greater than in persons without metastasis (35–38). Low IgG levels have been linked to a poor prognosis (35).
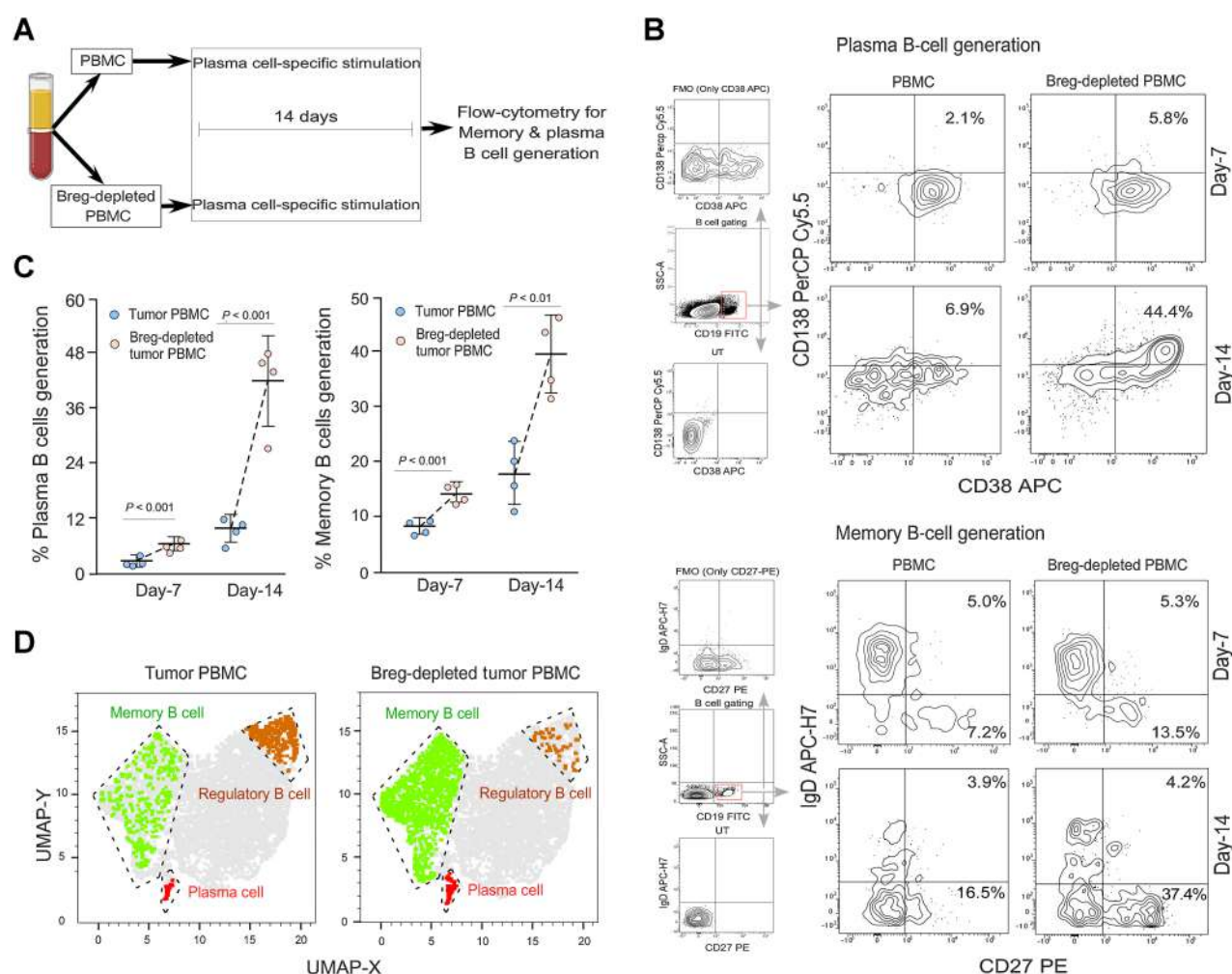
Figure 6.
CD19^{+}CD39^{-} Breg cells limit antibody responses by preventing memory to plasma B-cell differentiation. **A,** Schematic representation of memory and plasma B-cell generation. **B,** Flow-cytometric representation of plasma and memory B-cell generation when tumor PBMC's and Breg-depleted tumor PBMC's were specifically treated with plasma cell–specific induction (CD40LG+IL2+IL10). **C,** The bar chart shows the effect of CD19^{+}CD39^{-} Breg cells on the generation of memory and plasma B cells. Values are the mean ± SD of 4 sets of independent experiments obtained from different samples. **D,** A UMAP analysis sums up an inverse correlation between the memory (light green), plasma (red), and Breg-cell (orange) subsets in the peripheral circulation of patients with breast cancer and Breg cell–depleted conditions. All these three subsets obtained from two conditions (total PBMC and Breg cell–depleted PBMC) are overlayed on B cells (light grey). Student t test was used for all statistical analysis in Fig. 6 and all the error bars are represented as mean ± SD.

719 To investigate the reasons for this, we looked at the B-cell atlas
720 and noticed that in the blood of patients with breast cancer there was
721 an increase in the IL10-secreting transitional CD19^{+}CD24^{hi}CD38^{hi}
722 Breg-cell population, which have immunosuppressive properties
723 and showed an inverse relationship with switched memory
724 and antibody-producing plasma B cells. The inverse correlation
725 between memory and Breg cells has also been reported in pediatric
726 immune thrombocytopenia (39). This information suggested the
727 possibility that transitional Breg cells have a negative impact on B-
728 cell differentiation and antibody-mediated immunity. To test this
729 hypothesis, we needed to isolate viable CD19^{+}CD24^{hi}CD38^{hi} Breg
730 cells. However, these markers have limitations for isolating functional
731 Breg cells because they comprise three highly expressed cell surface
732 markers, leaving flow sorting as the only option. Unfortunately, as the
733 cell numbers are lower and they have to pass through the laser, it is
734 extremely difficult to acquire sufficient unstressed live Breg cells.

736 High-dimensional flow cytometry and microarray analysis helped
737 us to find CD19^{+}CD39^{-} as an alternate marker for CD19^{+}CD24^{hi}
738 CD38^{hi} B cells, allowing us to overcome this limitation. CD39 expres-
739 sion on the cell surface is strongly associated with mature B cells,
740 memory B cells, and plasma B cells. CD39-negativity, on the other
741 hand, is not linked to any of the above subsets, except for transitional B
742 cells that are CD19^{+}CD24^{hi}CD38^{hi}. CD39 is an E-NTPDase that
743 hydrolyzes ATP to ADP/AMP and finally to adenosine by CD73 from
744 activated B cells (40). The released adenosine binds to the B cells and
745 helps in differentiation into class-switched B cells (41). So, it can be
746 assumed that in the absence of any of these cell-surface molecules,
747 CD39 and CD73 or if the pathway is blocked, adenosine synthesis may
748 be hindered, resulting in impaired CSR. Consistent with the fact that
749 our identified Breg cells lack CD39, we observed that these cells
750 produce less adenosine than CD39^{+} B cells and that addition of
751 exogenous adenosine could restore the CSR events in B cells. As a
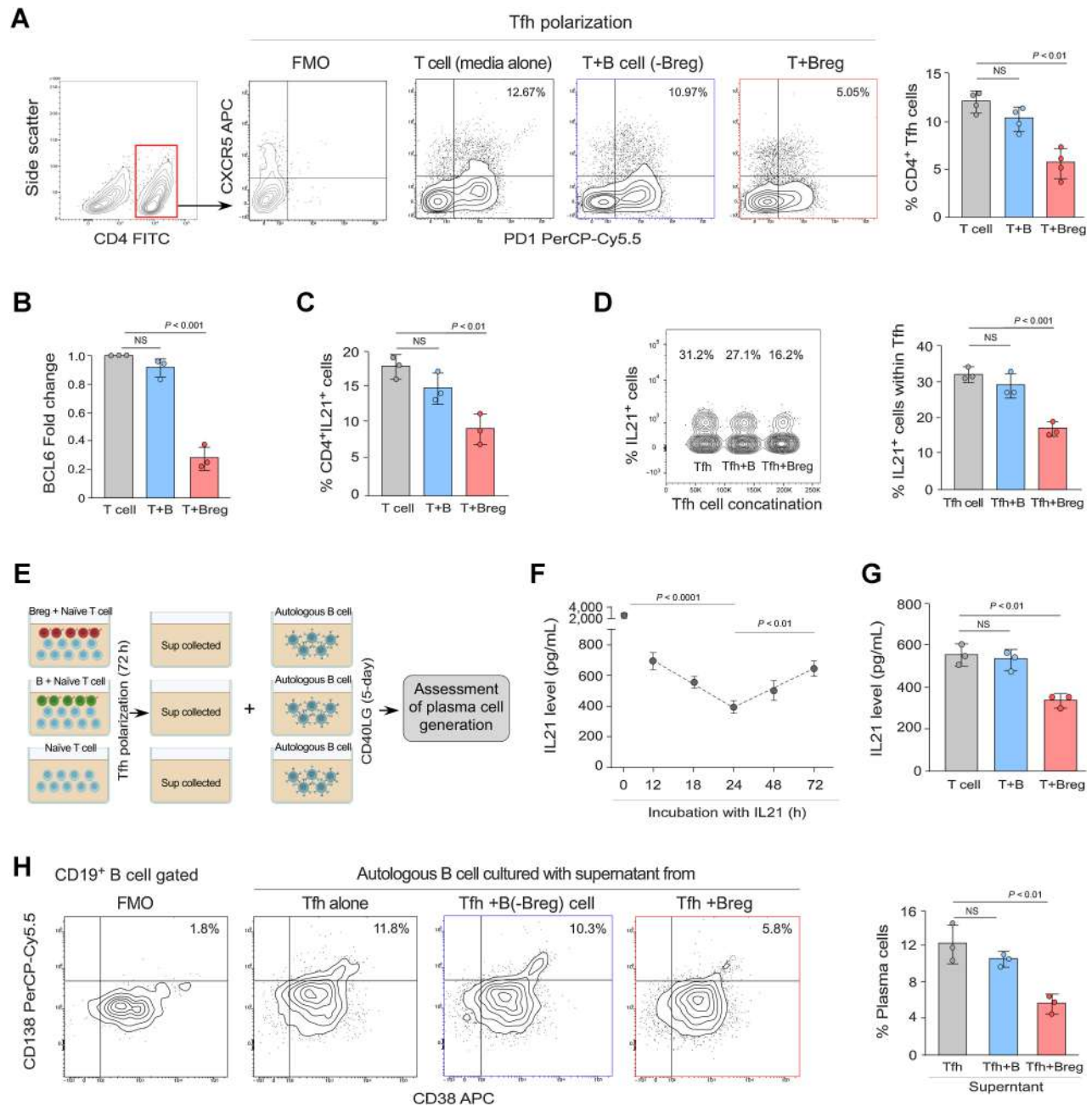
Figure 7.
Breg cells inhibit Tfh-cell differentiation and IL21 generation. **A,** Isolated human Breg cells or B cells (-Breg) from the peripheral circulation of tumor patients cocultured with autologous naïve CD4$^+$ T cells under Tfh cell–polarizing conditions. Tfh-cell differentiation was analyzed using flow cytometry (left). Results from multiple experiments are represented as ± SDM ($n = 4$; right). **B,** Real-time PCR data demonstrate *BCL6* expression from the above-mentioned culture conditions ($n = 3$). **C,** A bar graph ($n = 3$) depicts the percentage of CD4$^+$IL21$^+$ T cells cultured alone or with B cells or Breg cells (all subsets are isolated from tumor patient PBMC). Values are obtained from flow cytometry and represented as values mean ± SD. **D,** Percentage of IL21 expression among already differentiated Tfh cells cultured alone or with B cells/Breg cells is shown in a representative flow-cytometry concatenated plot. Cumulative results ($n = 3$) are represented in a bar graph as ± SDM. **E,** A schematic illustration of a culture condition in which ongoing Tfh differentiated cells were cultured with autologous Breg cells or B cells isolated from tumor patient PBMC for 72 hours and the collected cell supernatant was cultured with the same patient-derived unstimulated B cells (depleted of Breg cells) for another 5 days to assess plasma cell generation. **F,** ELISA was used to detect the time-dependent secretion of IL21 from ongoing generated Tfh cells that were initially treated with 5,000 pg/mL of recombinant IL21 protein. **G,** Naïve T cells are cultured alone or with B cells or Breg cells under Tfh cell–polarizing conditions for 72 hours (all subsets are isolated from tumor patient PBMC, $n = 3$). Supernatants are collected and are tested for the presence of IL21 by ELISA. The data are shown as mean ± SD. **H,** Generated plasma cells ($n = 3$) from the above-mentioned conditions (e) were represented with a flow-cytometry plot. Every culture experiment of T cell in presence of B cell indicate Bcell (-Breg) cell in case of Fig. 7. Student *t* test was used for all statistical analysis in Fig. 7 and all the error bars are represented as mean ± SD.

754 result of a greater number of CD39⁻ Breg cells failing to produce
755 adenosine in tumor, cannot assist themselves or other B cells in class
756 switching.

757 We determined that the IL10-producing $CD19^+CD39^-$ tumor-
758 associated Breg cells we identified are a stable, self-contained popu-
759 lation and do not re-differentiate. These Breg cells perform a variety
760 of immunoregulatory functions including inhibiting T helper–cell
761 proliferation, type-1 cytokine production, and T effector–cell survival,
762 and inducing the generation of $CD4^+FOXP3^+$ Treg cells. Studies
763 indicate that IL10 is a characteristic molecule of transitional Breg cells
764 that binds to T cells and promotes immunosuppression (13). TGFβ,
765 another immunosuppressive molecule, has little to no effect on
766 the suppressive action of Breg cells because its expression by Breg
767 cells is similar to that of non-Breg populations. Several studies
768 have revealed that interactions of CD80/CD86 on Breg cells with
769 CD28/CTLA4 on $CD4^+$ T cells work synergistically to release IL10
770 from B cells, suppressing T-cell pro-inflammatory cytokine produc-
771 tion (13, 42). PD-L1 expressed by Breg cells, which can bind to PD-1 on
772 T cells, also limits T helper–cell responses (43, 44). All of these
773 immunosuppressive processes in patients with cancer convert the
774 environment from immunogenic to tolerogenic, which helps the
775 tumor to grow more aggressively.

776 To test the possibility that Breg cells have a negative impact on
777 antibody responses, we depleted Breg cells from the PBMCs of patients
778 with breast cancer. Breg depletion resulted in substantial formation of
779 germinal transcripts and expression of AID, which is involved in
780 H-CSR, and differentiation of B cells into class-switched memory and
781 antibody-producing plasma B cells. It is well established that Tfh cells
782 play an important role in the establishment of germinal centers (32, 33).
783 Breg cells were found to have a negative impact on Tfh-cell generation
784 and IL21 production. As Breg cells prevent CSR by inhibiting the Tfh/
785 IL21 axis, long-lived plasma cell generation is halted, resulting in lower
786 IgG and a higher fraction of B cells unable to undergo CSR events,
787 resulting in higher IgM. Furthermore, CD39⁻ transitional B cells
788 (abundant in patients with cancer) produce high-IgM/low-IgG
789 because they do not participate in CSR due to their lower adeno-
790 sine-generating capacity. The combined effects of Breg cells on Tfh
791 cells and on adenosine levels might be the cause of the cancer patient's
792 high-IgM/low-IgG event. In this regard, it is worth noting that the
793 molecule(s) responsible for Breg cell–mediated suppression is still
794 under investigation. PD-L1 could be the molecule expressed by Breg
795 cells that prevents class-switching. PD-L1 may bind to PD-1 on Tfh
796 cell, inhibiting IL21 production and impairing both memory and
797 plasma B cell development (44). In-depth studies using single-cell
798 genomics and conditional-knockout mouse models may provide more

800 insight into the impact of Breg cells in B cell–mediated immune
801 regulation during tumor progression.

802 Our current work suggests that $CD19^+CD39^-$ is a key signature
803 surface-marker for tumor-associated IL10⁺ Breg cells, and their
804 augmentation in patients with breast cancer restricts Tfh-cell expan-
805 sion and IL21 secretion, hence inhibiting CSR during antibody
806 responses (Supplementary Fig. S8). Breg-cell depletion could, there-
807 fore, be a promising future strategy for enhancing the magnitude of
808 antibody responses and the dynamics of memory and plasma B cell–
809 mediated cancer immunotherapy.

Authors' Disclosures

Authors' Contributions

816 **S. Pati:** Conceptualization, formal analysis, validation, investigation, methodol-
817 ogy, writing–original draft. **S. Mukherjee:** Visualization, methodology. **S. Dutta:**
818 Methodology. **A. Guin:** Methodology, writing–review and editing. **D. Roy:** Meth-
819 odology. **S. Bose:** Methodology. **S. Paul:** Writing–review and editing. **S. Saha:**
820 Software, visualization. **S. Bhattacharyya:** Conceptualization. **P. Datta:** Clinical
821 sample providers. **J. Chakraborty:** Clinical sample providers. **D.K. Sarkar:** Clinical
822 sample providers. **G. Sa:** Conceptualization, resources, formal analysis, supervision,
823 funding acquisition, methodology, writing–original draft, project administration,
824 writing–review and editing.

Acknowledgments

Note

References

844 1. Andreu P, Johansson M, Affara NI, Pucci F, Tan T, Junankar S, et al.
845 FcRgamma activation regulates inflammation-associated squamous carcino-
846 genesis. Cancer Cell 2010;17:121–34.
847 2. Schmidt M, Böhm D, von Törne C, Steiner E, Puhl A, Pilch H, et al. The humoral
848 immune system has a key prognostic impact in node-negative breast cancer.
849 Cancer Res 2008;68:5405–13.
850 3. Cyster JG, Allen CDC. B-cell responses: cell interaction dynamics and decisions.
851 Cell 2019;177:524–40.
852 4. Barbera-Guillem E, Nelson MB, Barr B, Nyhus JK, May KF, Feng L, et al. B
853 lymphocyte pathology in human colorectal cancer. Experimental and clinical
854 therapeutic effects of partial B-cell depletion. Cancer Immunol Immunother
855 2000;48:541–9.
856 5. Bodagai M, Lee Chang C, Wejksza K, Lai J, Merino M, Wersto RP, et al. Anti-
857 CD20 antibody promotes cancer escape via enrichment of tumor-evoked

859 regulatory B cells expressing low levels of CD20 and CD137L. Cancer Res
860 2013;73:2127–38.
861 6. Mauri C, Menon M. The expanding family of regulatory B cells. Int Immunol
862 2015;27:479–86.
863 7. Sarvaria A, Madrigal JA, Saudemont A. B-cell regulation in cancer and antitumor
864 immunity. Cell Mol Immunol 2017;14:662–74.
865 8. Rosser EC, Mauri C. Regulatory B cells: origin, phenotype, and function.
866 Immunity 2015;42:607–12.
867 9. Ding T, Yan F, Cao S, Ren X. Regulatory B cell: new member of immunosup-
868 pressive cell club. Hum Immunol 2015;76:615–21.
869 10. Bigot J, Pilon C, Matignon M, Grondin C, Leibler C, Aissat A, et al. Transcrip-
870 tomic signature of the CD24ʰⁱ CD38ʰⁱ transitional B cells associated with an
871 immunoregulatory phenotype in renal transplant recipients. Am J Transplant
872 2016;16:3430–42.

11. Zha B, Wang L, Liu X, Liu J, Chen Z, Xu J, et al. Decrease in proportion of CD19+ CD24(hi) CD27+ B cells and impairment of their suppressive function in Graves' disease. PLoS One 2012;7:e49835.

12. Mauri C, Bosma A. Immune regulatory function of B cells. Annu Rev Immunol 2012;30:221–41.

13. Blair PA, Noreña LY, Flores-Borja F, Rawlings DJ, Isenberg DA, Ehrenstein MR, et al. CD19(+)CD24(hi)CD38(hi) B cells exhibit regulatory capacity in healthy individuals but are functionally impaired in systemic Lupus Erythematosus patients. Immunity 2010;32:129–40.

14. Shang J, Zha H, Sun Y. Phenotypes, functions, and clinical relevance of regulatory B cells in cancer. Front Immunol 2020;1:582657.

15. Mauri C. Novel frontiers in regulatory B cells. Immunol Rev 2021;299:5–9.

16. Peng B, Ming Y, Yang C. Regulatory B cells: the cutting edge of immune tolerance in kidney transplantation. Cell Death Dis 2018;9:109.

17. Olkhanud PB, Damdinsuren B, Bodogai M, Gress RE, Sen R, Wejksza K, et al. Tumor-evoked regulatory B cells promote breast cancer metastasis by converting resting CD4+ T cells to T-regulatory cells. Cancer Res 2011; 71:3505–15.

18. Wang WW, Yuan XL, Chen H, Xie GH, Ma YH, Zheng YX, et al. CD19+CD24hiCD38hiBregs involved in downregulate helper T cells and upregulate regulatory T cells in gastric cancer. Oncotarget 2015;6:33486–99.

19. Krämer A, Green J, Pollard J, Tugendreich S. Causal analysis approaches in Ingenuity Pathway Analysis. Bioinformatics 2014;30:523–30.

20. Saeed AI, Sharov V, White J, Li J, Liang W, Bhagabati N, et al. TM4: a free, open-source system for microarray data management and analysis. BioTechniques 2003;34:374–8.

21. Antohe M, Nedelcu RI, Nichita L, Popp CG, Cioplea M, Brinzea A, et al. Tumor-infiltrating lymphocytes: the regulator of melanoma evolution. Oncol Lett 2019; 17:4155–61.

22. Erdag G, Schaefer JT, Smolkin ME, Deacon DH, Shea SM, Dengel LT, et al. Immunotype and immunohistologic characteristics of tumor-infiltrating immune cells are associated with clinical outcome in metastatic melanoma. Cancer Res 2012;72:1070–80.

23. Largeot A, Pagano G, Gonder S, Moussay E, Paggetti J. The B-side of cancer immunity: the underrated tune. Cells 2019;8:E449.

24. Mauri C, Menon M. Human regulatory B cells in health and disease: therapeutic potential. J Clin Invest 2017;127:772–9.

25. Flores-Borja F, Bosma A, Ng D, Reddy V, Ehrenstein MR, Isenberg DA, et al. CD19+CD24hiCD38hi B cells maintain regulatory T cells while limiting TH1 and TH17 differentiation. Sci Transl Med 2013;5:173ra23.

26. Jin L, Weiqian C, Lihuan Y. Peripheral CD24hi CD27+ CD19+ B cells subset as a potential biomarker in naïve systemic lupus erythematosus. Int J Rheum Dis 2013;16:698–708.

27. Piper CJM, Rosser EC, Oleinika K, Nistala K, Krausgruber T, Rendeiro AF, et al. Aryl hydrocarbon receptor contributes to the transcriptional program of IL10-producing regulatory B cells. Cell Rep 2019;29:1878–92.

28. Glass DR, Tsai AG, Oliveria JP, Hartmann FJ, Kimmey SC, Calderon AA, et al. An integrated multi-omic single-cell atlas of human B-cell identity. Immunity 2020;53:217–32.

29. Figueiró F, Muller L, Funk S, Jackson EK, Battastini AMO, Whiteside TL. Phenotypic and functional characteristics of CD39high human regulatory B cells (Breg). Oncoimmunology 2016;5:e1082703.

30. Gould HJ, Beavil RL, Vercelli D. IgE isotype determination: epsilon-germline gene transcription, DNA recombination and B-cell differentiation. Br Med Bull 2000;56:908–24.

31. Shi Y, Agematsu K, Ochs HD, Sugane K. Functional analysis of human memory B-cell subpopulations: IgD+CD27+ B cells are crucial in secondary immune response by producing high affinity IgM. Clin Immunol 2003;108:128–37.

32. Nurieva RI, Chung Y, Hwang D, Yang XO, Kang HS, Ma L, et al. Generation of T follicular helper cells is mediated by interleukin-21 but independent of T helper 1, 2, or 17 cell lineages. Immunity 2008;29:138–49.

33. Vogelzang A, McGuire HM, Yu D, Sprent J, Mackay CR, King C. A fundamental role for interleukin-21 in the generation of T follicular helper cells. Immunity 2008;29:127–37.

34. Yuen GJ, Demissie E, Pillai S. B lymphocytes and cancer: a love–hate relationship. Trends Cancer 2016;2:747–57.

35. Saito H, Miyatani K, Kono Y, Murakami Y, Kuroda H, Matsunaga T, et al. Decreased serum concentration of total IgG is related to tumor progression in gastric cancer patients. Yonago Acta Med 2017;60:119–25.

36. Roberts MM, Bathgate EM, Stevenson A. Serum immunoglobulin levels in patients with breast cancer. Cancer 1975;36:221–4.

37. Roberts MM, Bass EM, Wallace IW, Stevenson A. Local immunoglobulin production in breast cancer. Br J Cancer 1973;27:269–75.

38. Tsuda B, Miyamoto A, Yokoyama K, Ogiya R, Oshitanai R, Terao M, et al. B-cell populations are expanded in breast cancer patients compared with healthy controls. Breast Cancer 2018;25:284–91.

39. Fang J, Lin L, Lin D, Zhang R, Liu X, Wang D, et al. The imbalance between regulatory memory B cells reveals possible pathogenesis involvement in pediatric immune thrombocytopenia. Hematology 2019;24:473–9.

40. Antonioli L, Pacher P, Vizi ES, Haskó G. CD39 and CD73 in immunity and inflammation. Trends Mol Med 2013;19:355–67.

41. Schena F, Volpi S, Faliti CE, Penco F, Santi S, Proietti M, et al. Dependence of immunoglobulin class-switch recombination in B cells on vesicular release of ATP and CD73 ectonucleotidase activity. Cell Rep 2013;3:1824–31.

42. Zhang Y, Gallastegui N, Rosenblatt JD. Regulatory B cells in antitumor immunity. Int Immunol 2015;27:521–30.

43. Zhao Y, Shen M, Feng Y, He R, Xu X, Xie Y, et al. Regulatory B cells induced by pancreatic cancer cell-derived interleukin-18 promote immune tolerance via the PD-1/PD-L1 pathway. Oncotarget 2018;9:14803–14.

44. Khan AR, Hams E, Floudas A, Sparwasser T, Weaver CT, Fallon PG. PD-L1hi B cells are critical regulators of humoral immunity. Nat Commun. Nature Publishing Group; 2015;6:5997.

AUTHOR QUERIES

AUTHOR PLEASE ANSWER ALL QUERIES

Q1:   Page: 1: Author: Per journal style, genes, alleles, loci, and oncogenes are italicized; proteins are roman. Please check throughout to see that the words are styled correctly. AACR journals have developed explicit instructions about reporting results from experiments involving the use of animal models as well as the use of approved gene and protein nomenclature at their first mention in the manuscript. Please review the instructions at http://aacrjournals.org/content/authors/editorial-policies#genenomen to ensure that your article is in compliance. If your article is not in compliance, please make the appropriate changes in your proof.

Q2:   Page: 1: Author: Please verify the drug names and their dosages used in the article.

Q3:   Page: 1: Author: Please verify the affiliations and their corresponding author links.

Q4:   Page: 1: Author: Please verify the corresponding author details.

Q5:   Page: 2: Author: Please define HBV.

Q6:   Page: 2: Author: Units of measurement have been changed here and elsewhere in the text from "M" to "mol/L," and related units, such as "mmol/L" and "μmol/L," in figures, legends, and tables in accordance with journal style, derived from the Council of Science Editors Manual for Authors, Editors, and Publishers and the Système international d'unités. Please note if these changes are not acceptable or appropriate in this instance.

Q7:   Page: 2: Author: Please define LPS.

Q8:   Page: 3: Author: Please expand PMA.

Q9:   Page: 4: Author: Please define SDM.

Q10:   Page: 5: Author: Please confirm quality/labeling of all images included within this article. Thank you.

Q11:   Page: 14: Author: The Authors' Disclosures statement that appears in the proof incorporates the information from forms completed and signed off on by each individual author. No factual changes can be made to disclosure information at the proof stage. However, typographical errors or misspelling of author names should be noted on the proof and will be corrected before publication. Please note if any such errors need to be corrected. Is the disclosure statement correct?

Q12:   Page: 14: Author: The contribution(s) of each author are listed in the proof under the heading "Authors' Contributions." These contributions are derived from forms completed and signed off on by each individual author. If you make changes to these contributions, you must inform the affected author(s).

AU: Below is a summary of the name segmentation for the authors according to our records. The First Name and the Surname data will be provided to PubMed when the article is indexed for searching. Please check each name carefully and verify that the First Name and Surname are correct. If a name is not segmented correctly, please write the correct First Name and Surname on this page and return it with your proofs. If no changes are made to this list, we will assume that the names are segmented correctly, and the names will be indexed as is by PubMed and other indexing services.

First Name	Surname
Subhadip	Pati
Sumon	Mukherjee
Saikat	Dutta
Aharna	Guin
Dia	Roy
Sayantan	Bose
Silpita	Paul
Sudipto	Saha
Sankar	Bhattacharyya
Pratyush	Datta
Jayati	Chakraborty
Diptendra K.	Sarkar
Gaurisankar	Sa

FOXP3/HAT1 Axis Controls Treg Infiltration in the Tumor Microenvironment by Inducing CCR4 Expression in Breast Cancer

Tania Sarkar[1†], Subhanki Dhar[1†], Dwaipayan Chakraborty[1], Subhadip Pati[1], Sayantan Bose[1], Abir K. Panda[1], Udit Basak[1], Sourio Chakraborty[1], Sumon Mukherjee[1], Aharna Guin[1], Kuladip Jana[1], Diptendra K. Sarkar[2] and Gaurisankar Sa[1*]

[1] *Division of Molecular Medicine, Bose Institute, Kolkata, India,* [2] *Department of Surgery, Institute of Post Graduate Medical Education & Research-Seth Sukhlal Karnani Memorial Hospital (IPGMER-SSKM) Hospital, Kolkata, India*

Infiltrating T-regulatory cells in the tumor microenvironment is a key impediment to immunotherapy and is linked to a poor prognosis. We found that tumor-infiltrating Tregs express a higher expression of the chemokine receptor CCR4 than peripheral Tregs in breast cancer patients. CCL22 and CCL17 are released by tumor cells and tumor-associated macrophages, attracting CCR4$^+$ Tregs to the tumor site. The Treg lineage-specific transcription factor FOXP3 changes the *CCR4* promoter epigenetically in conjunction with HAT1 to provide a space for FOXP3 binding and activation of the CCR4 gene. To increase CCR4 expression in Tregs, the FOXP3/HAT1 axis is required for permissive (K23 and K27) or repressive (K14 and K18) acetylation of histone-3. In murine breast and melanoma tumor models, genetic ablation of FOXP3 reduced CCR4$^+$ Treg infiltration and tumor size while also restoring anti-tumor immunity. Overexpression of FOXP3, on the other hand, increased CCR4$^+$ Treg infiltration, resulting in a decreased anti-tumor immune response and tumor progression. These findings point to FOXP3 playing a new role in the tumor microenvironment as a transcriptional activator of CCR4 and a regulator of Treg infiltration.

Keywords: Treg cells, FOXP3, CCR4, Treg infiltration, tumor microenvironment (TME)

INTRODUCTION

Tumor growth and development is a complex and dynamic process. Tumor microenvironment (TME), which is made up of a growing tumor mass, extracellular matrix, immune and stromal cells, and cell-secreted cytokines and chemokines, aids carcinogenesis (1). Growing tumor mass alters the immune system, resulting in a tolerogenic environment in the TME (2, 3). The development of

T-regulatory (Treg) cells is the most important and meaningful change among them. Among the diverse immune cells, Treg cells are critical components that play a major role in tumor immunological escape (4). Treg cells promote peripheral tolerance on the one hand, but their effects on tumor immunosurveillance are damaging on the other.

Tregs can arise spontaneously or in pathological conditions such as cancer from naïve or activated T cells. Natural Tregs (nTregs) develop in the thymus by stimulation of self-antigens (5). Tregs can also develop from naïve T cells during specific stimulation in the peripheral circulation (6). These Tregs are known as peripheral Tregs (pTregs) or induced Tregs (iTregs). iTreg cells phenotypically resemble nTregs (7). Tregs suppress the immune response in a variety of ways (8, 9). FOXP3 (forkhead F-box protein), an X-chromosome-encoded lineage-specific transcription factor, is necessary for Treg cells' suppressive functions (10, 11). FOXP3 activates or represses the transcription of its target genes to achieve its numerous tasks (12, 13). TGFβ is a key regulator of the signaling pathways that lead to Treg development by initiating and maintaining FOXP3 expression in $CD4^+CD25^-$ precursors (14). During tumor progression, Treg expansion decreases the function of tumor-specific T-effector (Teff) cells (12, 15, 16). Tregs are detected in high numbers in the peripheral blood and tumor tissue of patients, and a high number of Tregs is connected to a poor prognosis (13, 17).

Tregs, according to studies, infiltrate the tumor site from the peripheral circulation, creating an environment conducive to tumor progression; thus, they represent a key stumbling block in cancer treatment (18). Tregs decrease Teff cell and NK cell responses in cancer, interfering with both acquired and innate immunity (19). Tregs have a multitude of chemokine receptors that respond to chemokines released by the tumor mass as it grows. The interaction of chemokines and chemokine receptors on cell surfaces is required for its migration (20). As a result of chemokines generated by tumor cells, a concentration gradient is created, which Tregs follow to travel to the tumor site (21–23). The importance of the chemokine network in cancer is becoming increasingly clear. Treg compartmentalization and trafficking are tissue- and organ-specific, according to studies, and unique chemokine receptor expression leads to Treg selective retention and trafficking at regulatory locations. Tregs express the chemokine receptor CCR2 and interact with the ligand CCL2 as they move towards inflammatory tissue. CCR7–CCL19 interaction is also required for Treg trafficking to lymph nodes (24). Tregs, on the other hand, express a specific chemokine receptor, CCR4 (CD194), during metastasis (25). CCR4 is a chemokine receptor that Th2 cells, Treg cells, and skin-homing effector/memory T cells all express in different ways (26). CCR4, which binds to macrophage-derived chemokine (MDC/CCL22) and thymus- and activation-regulated chemokine (TARC/CCL17), is predominantly expressed by tumor-associated Treg cells (27, 28).

Both CCL22 and CCL17, which are produced by tumor cells, tumor-associated macrophages, and dendritic cells, establish a concentration gradient around the tumor mass and attract $CCR4^+$ Tregs to maintain immunological homeostasis in the tumor vicinity (29–31). When CCL22/CCL17 interacts with CCR4, a signaling cascade occurs, causing changes in cell shape and increased motility in Tregs, allowing them to infiltrate the TME (32). These tumor Tregs are functionally suppressive, capable of inhibiting tumor-specific immunity, promoting tumor development, and predicting poor prognosis (33). The importance of Treg tumor infiltration is well known, as Tregs make the TME tolerogenic and also reduce the effectiveness of anti-cancer therapy (34). The use of a humanized anti-CCR4 antibody (mogamulizumab) for the treatment of adult T cell leukemia and cutaneous T-cell lymphoma has recently been licensed, highlighting the importance of CCR4 in tumor growth (35, 36). However, little is known regarding *CCR4* transcriptional regulation in Treg cells in breast cancer. Our current research focuses on CCR4 modulation in Tregs and its implications for breast cancer.

Our research identifies a $FOXP3^+$ Treg population in tumor-infiltrating $CD4^+$ lymphocytes that are largely $CCR4^+$. The $FOXP3^+CCR4^+$ Tregs from breast cancer patients' peripheral circulation infiltrate tumor site in response to TME-secreted CCL17 and CCL22. The lineage-specific transcription factor FOXP3 controls its target genes in Treg cells (9), which led to the hypothesis that FOXP3 might also operate as a transcriptional regulator of CCR4. Genome-wide analysis of FOXP3-binding sites revealed that FOXP3 can act both as a transcriptional activator and as a repressor (37). Our predicted docking module suggests that the *CCR4* promoter has a FOXP3 responsive element. FOXP3 and HAT1 (Histone acetyl transferase-1) were shown to modify the *CCR4* promoter epigenetically to create a space for FOXP3 binding to transcriptionally activate the *CCR4* gene. Interference with FOXP3 binding to the *CCR4* promoter reduces Treg infiltration in the tumor site, reactivating the suppressed anti-tumor immune response. Understanding *CCR4's* transcriptional regulation will lead to novel approaches to prevent Treg infiltration in tumors. According to current research, it will soon be discovered as a technique to improve the immune system's response to tumors.

MATERIALS AND METHODS

Patients

The participants in this study were 23 female breast cancer patients (Stage I, $n = 6$; Stage II, $n = 8$; Stage III and IV, $n = 9$; ages: 18–65 years) and 10 age-/sex-matched healthy people (**Table S1**). The tumor stage was assessed using the TNM classification of the International Union Against Cancer from 2002. Three patients with Stage II breast cancer who had mastectomy were given ipsilateral normal breast tissues. The ethics committees of the ESI Post-Graduate Institute of Medical Science and Research, Kolkata (Approval No: ESI-PGIMSR/MKT/IEC/13/2017 dated December 22, 2017), the Institute of Post-Graduate Medical Education and Research Oversight

Committee (Approval No. IPGME/IEC/13/2017 dated December 22, 2017), and Human Ethics Committee, Bose Institute (Approval No: BIHEC/2017-18/7, dated May 28, 2017) approved the collection of post-operative breast tumor tissue samples and peripheral blood from breast cancer patients/ normal. All patients enrolled in the trial gave their informed consent.

T Cell Isolation and Culture

To obtain PBMC, peripheral blood was centrifuged at $800 \times g$ for 45 min over the lymphocyte separation medium (Histopaque). For T-cell polarization, magnetic-bead sorted naïve $CD4^+CD45RA^+$ T cells from cord blood were activated with anti-CD3 and anti-CD28 beads (Invitrogen) before being allowed to develop into Tregs in the presence of recombinant TGFβ (5 ng/ml) and IL2 (50 U/ml) and anti-IFNγ antibody (PeproTech). Flow cytometry was used to determine the purity of the enhanced cells, which was consistently >90%. During flow cytometric analysis, LymphoGate was employed to detect lymphocytes. Treg differentiation was confirmed by flow cytometry and qPCR. Cells were cultured in a complete RPMI-1640 medium supplemented with 10% FBS at 37°C in a humidified 5% CO_2 incubator. All experiments were performed with mycoplasma-free cells.

THP1 Culture

THP1 (CVCL 0006), a well-established monocyte cell line, was grown in RPMI-1640 with 10% serum. Monocytes were treated with PMA (5 ng/ml; Sigma) to generate the M-M0 subtype. THP1 can be polarized from Mϕ-M0 to Mϕ-M1 by adding LPS (100 ng/ml; Peprotech) and IFNγ (20 ng/ml; PeproTech) to it. Mϕ-M0 was also polarized to the Mϕ-M2 subtype by treating it with IL4 (20 ng/ml; PeproTech) for 48 h. The cell line has been authenticated using STR (or SNP) profiling within the last 3 years by the National Centre for Cell Science, Pune, India. All experiments were performed on mycoplasma-free cells.

Ex Vivo Tumor Microenvironment

To generate ex vivo TME, tumor tissues were collected from breast cancer patients undergoing surgical procedures, minced, and stirred in cell dissociation reagent containing collagenase Type IV in DMEM/F-12 for 2 h. The tumor cell suspension was filtered through nylon mesh and centrifuged for 10 min at $250 \times g$. To make a single-cell suspension, the cell pellet was washed with serum-free RPMI 1640 and resuspended in complete RPMI 1640 media. CD24 and ESA positivity or CD4-/CD8- and CD25 negativity were used to assess the purity of those cells flow cytometrically. T cells from healthy volunteers were over-layered on top of primary breast tumor cells (to mimic the TME in vitro) and cultured for 72 h to generate Tregs ex vivo (**Figure S1**) (38).

Flow Cytometry and Cell Sorting

Fluorophore-conjugated CD4 (FITC/-PE), CD25 (PE/PE-CY7), CD127 (AF-647), CTLA4 (PE), FOXP3 (AF-647), and CCR4 (BV-421/PE) antibodies (Biolegend/BD Bioscience) were used to stain cells for phenotyping. The expression of Th1- and Th2-specific transcription factors T-bet (Santa Cruz) and GATA3 (Santa Cruz) was used to determine the percentage of Th1 and Th2 cells, respectively. Cells were stimulated for 5 h at 37°C with cell activation cocktail and brefeldin-A (Biolegend) before being stained with anti-IL10 (BV-421) using the Cytofix/CytoPerm Plus kit (BD Biosciences). The fluorescent-conjugated annexin-V was used to assess cellular apoptosis (BD Bioscience). For the purification of naïve and Treg cells, $CD4^+$ cells, labeled for CD45RA, CD25, and CTLA4, were subjected to high-speed cell sorting (FACS-ARIA, BD Biosciences) to obtain $CD25^+CTLA4^+$ Treg and $CD45RA^+$ naïve T cells. Data were acquired and analyzed by FACS using FACS-Suite and FlowJo software (BD Biosciences). Quadrants were constructed based on signals utilizing FMO and unstained controls to quantify stained cells in contour plots. For t-SNE analysis, the lymphocyte population was gated and the $CD4^+$ population was subsequently marked. The lymphocyte population from blood acquired from a breast cancer patient in the cohort was a down-sample with 5,000 cells, and the dimensionality reduction was done with the population to create t-SNE parameters.

Transduction

Ex vivo-generated Tregs (2×10^6 cells) were transduced with FOXP3-/CCR4-shRNA (Thermo-Fisher Scientific), FOXP3-/CCR4-cDNA (ADDGENE), or control vector by electroporation (Invitrogen, USA) in a single-pulsed method (voltage 260 V and capacitance 1050 µF). Transduced cells were cultured for 48 h before being exposed to downstream tests. We routinely achieved a transduction effectiveness of 85%–90% under these conditions without compromising cell viability.

cDNA Preparation and Real-Time PCR

Treg cells (2×10^6 cells) were stimulated with PMA and ionomycin for 4 h at 37°C before RNA was isolated using TRIzol reagent (Thermo Fisher Scientific) and reverse transcribed using Verso-cDNA synthesis kit (Thermo-Fisher Scientific). FastStart Essential DNA Green Master (Roche) was used for qPCR analysis, which was carried out using a GeneAmp PCR-2720 (Applied Biosystems, CA, USA). Melting curves using LC96 SW1.1 software were used to assess amplification products using SYBR-green detection (Roche). A $2^{-\Delta\Delta Ct}$ approach was used to analyze the data. The expression level of the house-keeping gene, GAPDH, was used to normalize for variations in the amount of RNA. The respective primers list is given in **Table S2**.

ChIP and Re-ChIP

To cross-link the protein–DNA complexes, ex vivo-generated Tregs (2×10^6 cells) were cross-linked in 1% p-formaldehyde for 15 min at 37°C. Soluble chromatin (7–20 µg) was treated with 4–5 µg of antibody overnight at 4°C after being sonicated and precleared with protein-A agarose/salmon-sperm DNA. FOXP3, RNA POL-II (Santa Cruz), HAT1, acetylated-H3 (K14, K18, K23, and K27), anti-rabbit, and anti-mouse immunoglobulin-G antibodies (Cell Signaling Technology) were used for ChIP and Re-ChIP assays. In addition, a negative control IgG (Sigma-Aldrich) was employed. Following immunoprecipitation and washing, DNA from each immunoprecipitation was measured

using distinct primer sets (**Table S2**) for the FOXP3 and RNA POL-II binding sites on the *CCR4* promoter by qPCR. After eliminating background immunoprecipitation assessed with nonspecific IgG or the input sample, the fold-change in occupancy of each protein at the *CCR4*-promoter region of Treg relative to the T naïve cell was estimated. DNA–protein complexes immunoprecipitated with anti-FOXP3 antibody in primary ChIP were eluted with 25 µl of 10 mM dithiothreitol for 30 min at 37°C and diluted 20 times with Re-ChIP buffer for the Re-ChIP tests (1% Triton X-100, 2 mM EDTA, 150 mM NaCl, and 20 mM Tris-HCl; pH 7.5). After that, the complexes were re-immunoprecipitated with anti-HAT1 antibody before qPCR examination of the precipitated chromatin DNA (39).

Confocal Microscopy

Breast tumor patient-derived Tregs and naïve T cells were washed in PBS with 1% BSA. Then 1×10^4 cells were allowed to adhere to poly-L-lysine-coated slides. Cells were fixed with 4% *p*-formaldehyde and permeabilized with 0.2% saponin. After blocking with 3% BSA, cells were incubated with anti-FOXP3-/-CCR4 (rabbit/mouse mAb), followed by fluorescence-tagged secondary antibodies (Invitrogen) and DAPI (BD Biosciences). Cells were visualized in Leica confocal microscope, with DPX mounting medium, at 60× magnification. Images were analyzed by ImageJ software (40).

Trans-Well Assay

Polycarbonate filters (pore size, 5 µm; Cell Culture Inserts, Corning) were used for Trans-well assay that helps direct the passage of the cells from the upper to the lower chamber. The upper chamber was plated with RPMI-1640 medium containing patient-derived Tregs and the lower chamber was plated with tumor cell supernatant containing recombinant CCL22 (PeproTech). After 4 h at 37°C, cells migrated at the lower chamber were collected, immunostained, and analyzed in a flow cytometer. To check the role of FOXP3 in Tregs migration, *ex vivo*-generated Tregs were first transfected with lentivirus containing desired clones and the transfected cells were placed in the upper chamber of trans-well plates.

Western Blot

Cells were homogenized in buffer (20 mM Hepes, pH 7.5, 10 mM KCl, 1.5 mM MgCl$_2$, 1 mM Na-EDTA, 1 mM EGTA, and 1 mM DTT) supplemented with protease and phosphatase cocktail inhibitor. A total of 60 µg of protein was resolved using 10% SDS-PAGE, transferred to nitrocellulose membrane, and probed with specific antibodies CCR4 (Santa Cruz) and FOXP3 (Santa Cruz). Secondary antibodies used (1:10,000) were conjugated with HRP (Sigma). After that, the immunoblots were developed by chemiluminescence method using luminol and coumaric acid. Equal protein loading was confirmed with anti-β-actin antibody (mAb) (Santa Cruz).

Lentivirus Preparation

Packaging of lentiviruses was performed by transient transfection of HEK cells. One day before transfection, HEK cells were seeded in a T75 flask at 1×10^5 cells/cm^2 in DMEM supplemented with 10% FCS, 1 mM pyruvate, and 40 mg/ml gentamicin. The calcium phosphate precipitation method was used to co-transfect cells using 7.5 µg of gag/pol packaging plasmid psPAX2, 7.5 µg of pGIPZ-Foxp3-shRNA/Foxp3-cDNA transfer vector, and 4 µg of envelope plasmid pMD2.G using the Profection mammalian transfection kit (Promega, USA). Transfections were carried out in 10 ml of DMEM without antibiotics, and the cells were grown for 16 h. After that, the medium was replaced with complete DMEM, and after 48 h, the supernatant was collected. Centrifugation at 1,500 rpm for 5 min at 4°C was used to remove cell debris, which was then passed through a 0.45-µm pore PES filter. For concentration, 20 ml of supernatant was centrifuged at 4,000 rpm for 20 min at 4°C in a 12% polyethylene glycol (PEG-8000) solution. In serum and antibiotic-free DMEM, pelted viruses were re-suspended and the aliquots were kept at −80°C for further use (41).

Animal Model

BALB/c and C57/BL6 mice weighing 20–25 g (in-house animal facility) were kept in a temperature-controlled environment with a light–dark cycle. All animal experiments were carried out following the National Institutes of Health's Principles of Laboratory Animal Care (NIH publication No. 85-23, revised in 1985) as well as Indian laws on "Animal Protection" under the provision of the Bose Institute Animal Ethics Committee for the control and supervision of animal experiments (Reg. No. 95/99/CPCSEA; Approval No: IAEC/BI/47/2017). A total of 2×10^6 isogenic mammary carcinoma 4T1 or B16/F10 melanoma cells (ATCC) were injected in the breast fat pad of BALB/c mice or subcutaneously in C57/BL6 mice, respectively. Mice were separated into five groups, each with three mice: (i) control, (ii) tumor alone (no transduction), (iii) control vector, (iv) Foxp3-shRNA, and (v) Foxp3-cDNA. The experiments were repeated twice. Lentivirus-bearing desired clones were injected into the tail vein after 7 days of tumor inoculation. Mice were tracked for the next 21 days. Every other day, the tumor volume was measured. The tumor volume was calculated using the formula V = (W2 × L)/2 (caliper measurements), where V represents the tumor volume, W represents the tumor width, and L represents the tumor length. After 21 days, the mice were sacrificed, and Tregs from PBMC and the tumor site location were examined using flow cytometry (42).

Bioinformatics and Statistical Analysis

The correlation study between FOXP3 and CCR4 was executed using R2: Genomics Analysis and Visualization Platform. The same dataset was used to construct t-SNE plots for FOXP3 and CCR4. MatInspector software was used to analyze the *CCR4* promoter. Multiple sequence alignments of *CCR4* promoter between human and mouse was done by Clustal W. Unless otherwise stated, values are shown as the standard error of the mean (SEM). A 2-way ANOVA was used to compare different experimental groups, followed by a post-hoc Bonferroni modification of the multiple comparison *t*-test. A Student's *t*-test was used to examine the significance of the differences between mean values when suitable. At $p < 0.05$, the results were considered significant. Graph Pad software was used to

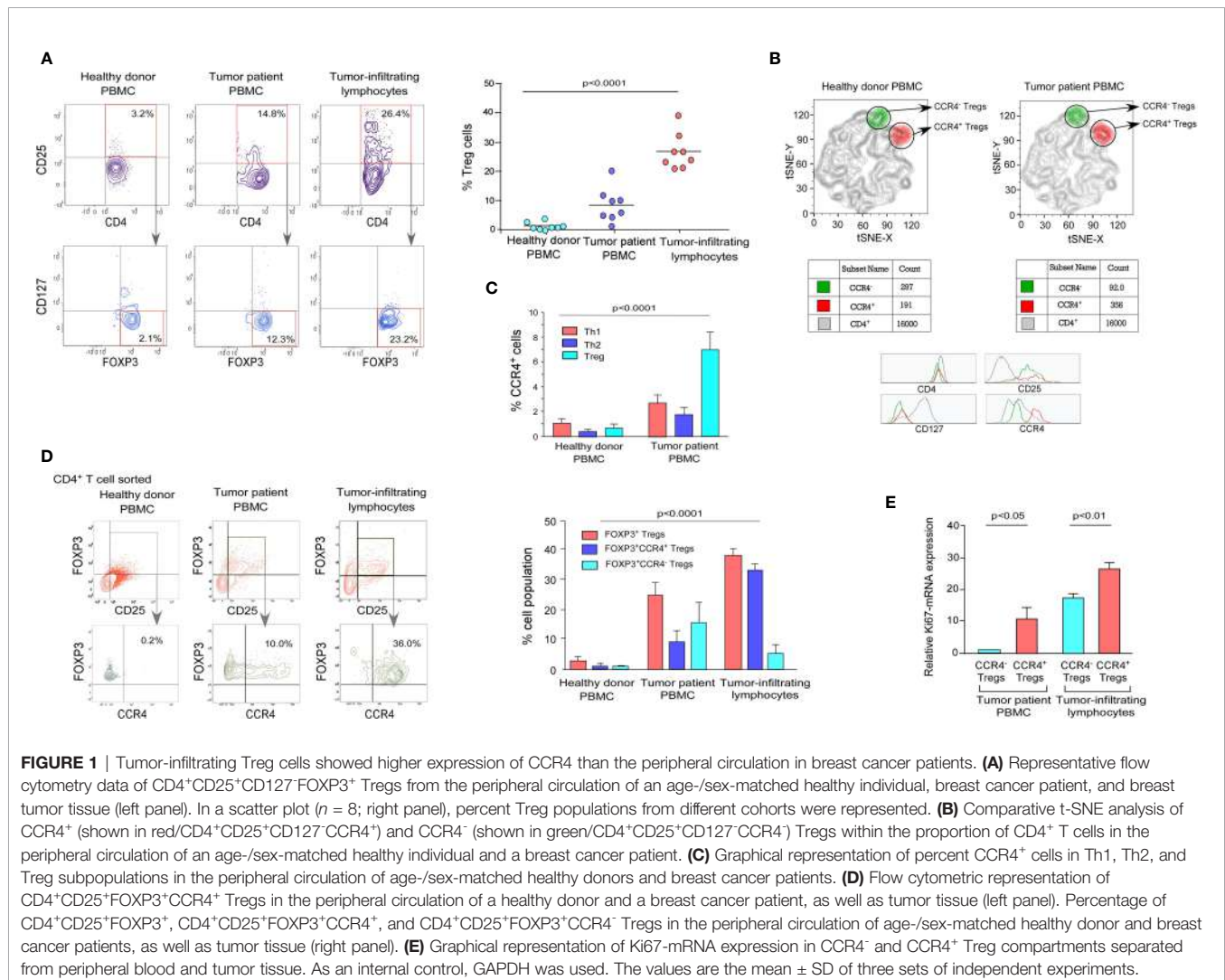create a heatmap for the fold-change values. Prism software was used to analyze the data (Graph Pad software).

RESULTS

Tumor-Infiltrating Treg Cells Showed Higher Expression of CCR4 Than the Peripheral Circulation in Breast Cancer Patients

We obtained peripheral blood and post-operative breast tumor tissue from a cohort of 8 breast cancer patients undergoing surgery to establish the expression pattern of CCR4 in Tregs. We used a mix of phenotypic markers to further characterize human Tregs and their relationship to tumor progression characteristics. FOXP3 was employed as an internal marker, while CD4, CD25, and CD127 were used as surface markers (33). In comparison to age-/sex-matched healthy donors, patients with advanced breast cancer had higher proportions of $CD4^+CD25^+CD127^-FOXP3^+$

Tregs in the peripheral circulation and tumor tissue, as shown in **Figure 1A** (**Figure 1A**; left panel). Based on the cell surface marker expression pattern, we chose $CD4^+CD25^+CD127^-$ as a suitable set of surface markers to sort Tregs for further characterization. The tumor site had a higher percentage of $CD4^+CD25^+CD127^-FOXP3^+$ Tregs than the peripheral circulation of breast cancer patients and age-/sex-matched healthy donors (**Figure 1A**; right panel).

CCR4 is a chemokine receptor that is selectively expressed by Tregs in various pathophysiological situations and plays an important role in lymphocyte organ-specific migration (35, 36). The distribution pattern of CCR4 in tumor-associated $CD4^+CD25^+CD127^-$ Treg populations in healthy donor and tumor patients was determined using a comparative t-SNE method based on multi-color flow cytometry data (**Figure 1B**). The two populations of Tregs ($CCR4^+$ and $CCR4^-$) are present in both healthy donors and tumor patients, according to CCR4 expression levels; however, the presence of the $CCR4^+$ Treg population is higher than the $CCR4^-$ Treg population in tumor patients, which indicates that Treg increases the expression of

FIGURE 1 | Tumor-infiltrating Treg cells showed higher expression of CCR4 than the peripheral circulation in breast cancer patients. **(A)** Representative flow cytometry data of $CD4^+CD25^+CD127^-FOXP3^+$ Tregs from the peripheral circulation of an age-/sex-matched healthy individual, breast cancer patient, and breast tumor tissue (left panel). In a scatter plot (n = 8; right panel), percent Treg populations from different cohorts were represented. **(B)** Comparative t-SNE analysis of $CCR4^+$ (shown in red/$CD4^+CD25^+CD127^-CCR4^+$) and $CCR4^-$ (shown in green/$CD4^+CD25^+CD127^-CCR4^-$) Tregs within the proportion of $CD4^+$ T cells in the peripheral circulation of an age-/sex-matched healthy individual and a breast cancer patient. **(C)** Graphical representation of percent $CCR4^+$ cells in Th1, Th2, and Treg subpopulations in the peripheral circulation of age-/sex-matched healthy donors and breast cancer patients. **(D)** Flow cytometric representation of $CD4^+CD25^+FOXP3^+CCR4^+$ Tregs in the peripheral circulation of a healthy donor and a breast cancer patient, as well as tumor tissue (left panel). Percentage of $CD4^+CD25^+FOXP3^+$, $CD4^+CD25^+FOXP3^+CCR4^+$, and $CD4^+CD25^+FOXP3^+CCR4^-$ Tregs in the peripheral circulation of age-/sex-matched healthy donor and breast cancer patients, as well as tumor tissue (right panel). **(E)** Graphical representation of Ki67-mRNA expression in $CCR4^-$ and $CCR4^+$ Treg compartments separated from peripheral blood and tumor tissue. As an internal control, GAPDH was used. The values are the mean ± SD of three sets of independent experiments.

CCR4 to infiltrate in the TME. We intended to evaluate the status of CCR4 expression in other T-cell subsets (Th1 and Th2) because Tregs show a higher expression of CCR4 in tumor settings. When compared to healthy donors, CCR4 expression is significantly increased by Tregs during tumor condition; however, CCR4 expression is not significantly increased by other T-cell subsets (**Figure 1C**).

We evaluated the expression level of CCR4 in both the peripheral circulation (source) and the tumor site (destination) since it is the tumor-specific migratory marker of Tregs. **Figure 1D** shows that the CCR4$^+$ Treg population was found in higher frequency in Tregs obtained from the tumor site (30%) than in Tregs obtained from the tumor patient's peripheral blood (10%), implying that when the Treg acquires CCR4 expression in the peripheral circulation, it migrates to the tumor site. The graphical representation (**Figure 1D**, right panel) also shows that CCR4$^+$ Tregs account for the majority of Tregs in tumor tissue, whereas the percentage in the peripheral circulation of both the healthy donor and the tumor patient is relatively low, indicating that only CCR4$^+$ Tregs can infiltrate the tumor site and CCR4$^-$ Tregs cannot (**Figure 1D**). In comparison to CCR4$^-$ Tregs, CCR4$^+$ Tregs from both the peripheral circulation and tumor tissue had greater Ki67 expression. CCR4$^+$ Tregs from both the peripheral blood and tumor tissue had greater Ki67 expression than CCR4$^-$ Tregs, indicating that CCR4$^+$ Tregs are more proliferative (**Figure 1E**). The tumor immune escape is facilitated by the eventual proliferation of these CCR4$^+$ Treg cells in tumor tissue.

Cell Surface Receptor CCR4 Interacts With Chemokine CCL22 and CCL17 to Migrate Treg Cells Into Tumor Microenvironment
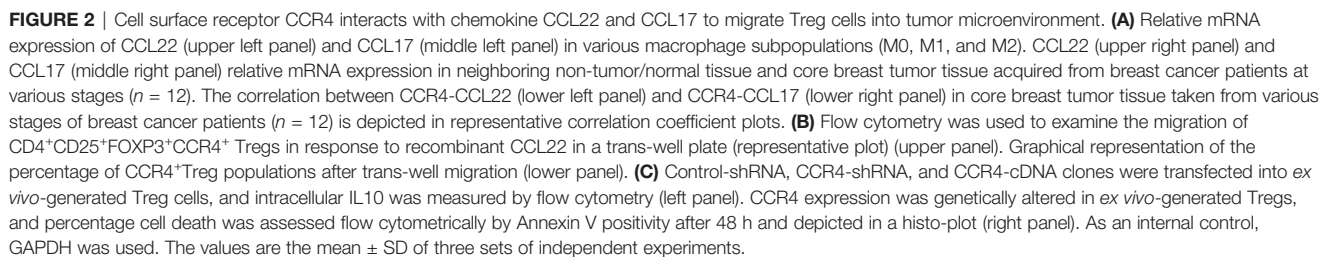
CCR4 is a chemokine receptor that responds to CCL22 and CCL17 ligands (27, 28). The interaction between CCL22/CCL17 and CCR4 triggers a signaling cascade in Tregs that results in changes in cell shape and increased motility. In our experiments, we discovered that only M2 macrophages (tumor-associated macrophages) present in the TME express higher levels of CCL22/CCL17 than other macrophage subsets (**Figure 2A**). **Figure S2** shows the validation of macrophage subtype characterization. It was also clear that core breast tumor tissue showed higher levels of CCL22/CCL17 transcripts than neighboring non-tumor/normal tissue (**Figure 2A**). We used correlation coefficient plots to show the relationship between CCR4 and CCL22/CCL17 expression in core breast tumor tissue, which revealed a strong positive connection between CCR4 and CCL22/CCL17 in breast tumor tissue (**Figure 2A**, lower panel). The ability of CCR4$^+$ Tregs to migrate towards the CCL22 chemokine gradient was assessed using a trans-well migration assay in which Tregs from breast cancer patient blood were placed at the top of the chamber and a gradient of recombinant CCL22 was adjusted in the lower chamber containing cell culture media. It was observed that as the concentration of CCL22 increased, the percentage of migrating CCR4$^+$ Tregs increased (**Figure 2B**). In the lower panel, a

graphical representation of the same has been provided (**Figure 2B**). CCL22 and CCL17 levels in breast cancer tissue are associated with strong Treg infiltration and consequent immunosuppression; hence, it could be used as a prognostic marker. Several studies have also found that Treg cells dampen the immune system by producing the immunosuppressive cytokine IL10 (12). As shown in **Figure 2C**, the alteration of CCR4 expression in Treg has no negative impact on its immunosuppressive function since the level of intracellular IL10 is not affected. Furthermore, the Annexin-V positivity test revealed that CCR4 expression does not confer a survival advantage to Tregs. All of this suggests that the chemokine receptor CCR4 is exclusively involved in the tumor-specific migration of Tregs without affecting its survival or suppressive activities.

FOXP3 Binds at the *CCR4* Promoter and Regulates CCR4 Expression in Treg Cells

We decided to investigate FOXP3's activity as a transcriptional activator for *CCR4* because it plays such an important role in Treg development and function (37). Being a transcription factor, FOXP3 binds to the promoter region of its target genes. Because FOXP3 nuclear localization is critical for Treg function, we decided to investigate its nuclear translocation. Our findings show that nuclear localization of FOXP3 is more common in tumor patients' lymphocytes than in normal lymphocytes (**Figure 3A**), implying that it plays a dynamic role as a transcription factor. Our t-SNE study of TCGA data from patients with breast invasive cancer reveals that high CCR4 expression in tumor tissue is linked to high FOXP3 expression (**Figures 3B, C**). With this in mind, we aimed to confirm the positive association between CCR4 and FOXP3 in other cohorts of breast cancer patients. To demonstrate the association between CCR4 and FOXP3 expression in core breast tumor tissue, we created a correlation coefficient plot, which further indicates that CCR4 expression is highly correlated with FOXP3 expression in breast tissue taken from different cohorts (**Figure 3D**).

We ablated or overexpressed FOXP3 in Treg cells and grew them on a breast tumor organoid bed to replicate the *ex vivo* TME to better understand the role of FOXP3 in *CCR4* transcriptional activation. Flow cytometry was used to confirm Treg production *ex vivo* (**Figure S1**). CCR4-mRNA expression is very low in FOXP3-ablated Tregs and very high in FOXP3-overexpressed Tregs, as seen in **Figure 3E**. After FOXP3 depletion/overexpression, CCR4 expression at the protein level as well as at the cell surface showed a consistent pattern with mRNA levels (**Figure 3F**). As a transcription factor, FOXP3 binds to the regulatory area of its target gene's promoter, prompting us to investigate FOXP3's binding site at the *CCR4* promoter. For the same reason, we used *in silico* analysis to examine the *CCR4* promoter and observed two FOXP3-binding sites at the −668 bp to −651 bp (distal site) and −124 bp to −108 bp (proximal site) regions of the promoter. **Figure 3G** shows the FOXP3 (DNA-binding domain) consensus promoter binding sequence (obtained from Jasper). This sequence is found in the regulatory region of all FOXP3 target genes; the *CCR4* promoter contains the same DNA-binding region, prompting us to

FIGURE 2 | Cell surface receptor CCR4 interacts with chemokine CCL22 and CCL17 to migrate Treg cells into tumor microenvironment. **(A)** Relative mRNA expression of CCL22 (upper left panel) and CCL17 (middle left panel) in various macrophage subpopulations (M0, M1, and M2). CCL22 (upper right panel) and CCL17 (middle right panel) relative mRNA expression in neighboring non-tumor/normal tissue and core breast tumor tissue acquired from breast cancer patients at various stages ($n = 12$). The correlation between CCR4-CCL22 (lower left panel) and CCR4-CCL17 (lower right panel) in core breast tumor tissue taken from various stages of breast cancer patients ($n = 12$) is depicted in representative correlation coefficient plots. **(B)** Flow cytometry was used to examine the migration of CD4$^+$CD25$^+$FOXP3$^+$CCR4$^+$ Tregs in response to recombinant CCL22 in a trans-well plate (representative plot) (upper panel). Graphical representation of the percentage of CCR4$^+$Treg populations after trans-well migration (lower panel). **(C)** Control-shRNA, CCR4-shRNA, and CCR4-cDNA clones were transfected into *ex vivo*-generated Treg cells, and intracellular IL10 was measured by flow cytometry (left panel). CCR4 expression was genetically altered in *ex vivo*-generated Tregs, and percentage cell death was assessed flow cytometrically by Annexin V positivity after 48 h and depicted in a histo-plot (right panel). As an internal control, GAPDH was used. The values are the mean ± SD of three sets of independent experiments.

investigate FOXP3's binding to the *CCR4* promoter. The *in silico* finding was validated by ChIP analysis. FOXP3 binding at the distal site was stronger than at the proximal position (**Figure 3G**), showing that the distal region is the most critical FOXP3-binding site in the *CCR4* promoter. We also examined RNA POL-II binding on the *CCR4* promoter to confirm that the promoter region was open for FOXP3 binding, and the ChIP signal for RNA POL-II was highest in this region (**Figure 3G**).

The FOXP3/HAT1 Axis Epigenetically Alters *CCR4* Promoter to Promote Treg Infiltration in the Tumor Site

We altered FOXP3 in *ex vivo*-generated Tregs to better understand the processes through which FOXP3 modulates *CCR4* transcription. We found that ablation of FOXP3 decreased the promoter binding, but overexpression of FOXP3 boosted it (**Figure 4A**). Because of the permissive and repressive deacetylation state of histone-3 in naïve T cells, the *CCR4* promoter stays inaccessible. FOXP3 overexpression increased HAT1 binding to the *CCR4* promoter's distal regions, modifying the chromatin structure and making it accessible to FOXP3 (**Figures 4B, C**). Interestingly, both FOXP3 and HAT1 binding is required for permissive (K23 and K27) or repressive (K14 and K18) acetylation of histone-3 in Tregs to increase CCR4 expression. **Figure 4D** shows a schematic depiction of the FOXP3-binding region on the *CCR4* promoter at the distal region coupled with HAT1. FOXP3 expression in Tregs was ablated or overexpressed by genetic manipulation, and the ability of the altered Tregs to migrate was monitored using a trans-well migration assay in the presence of recombinant CCL22 to
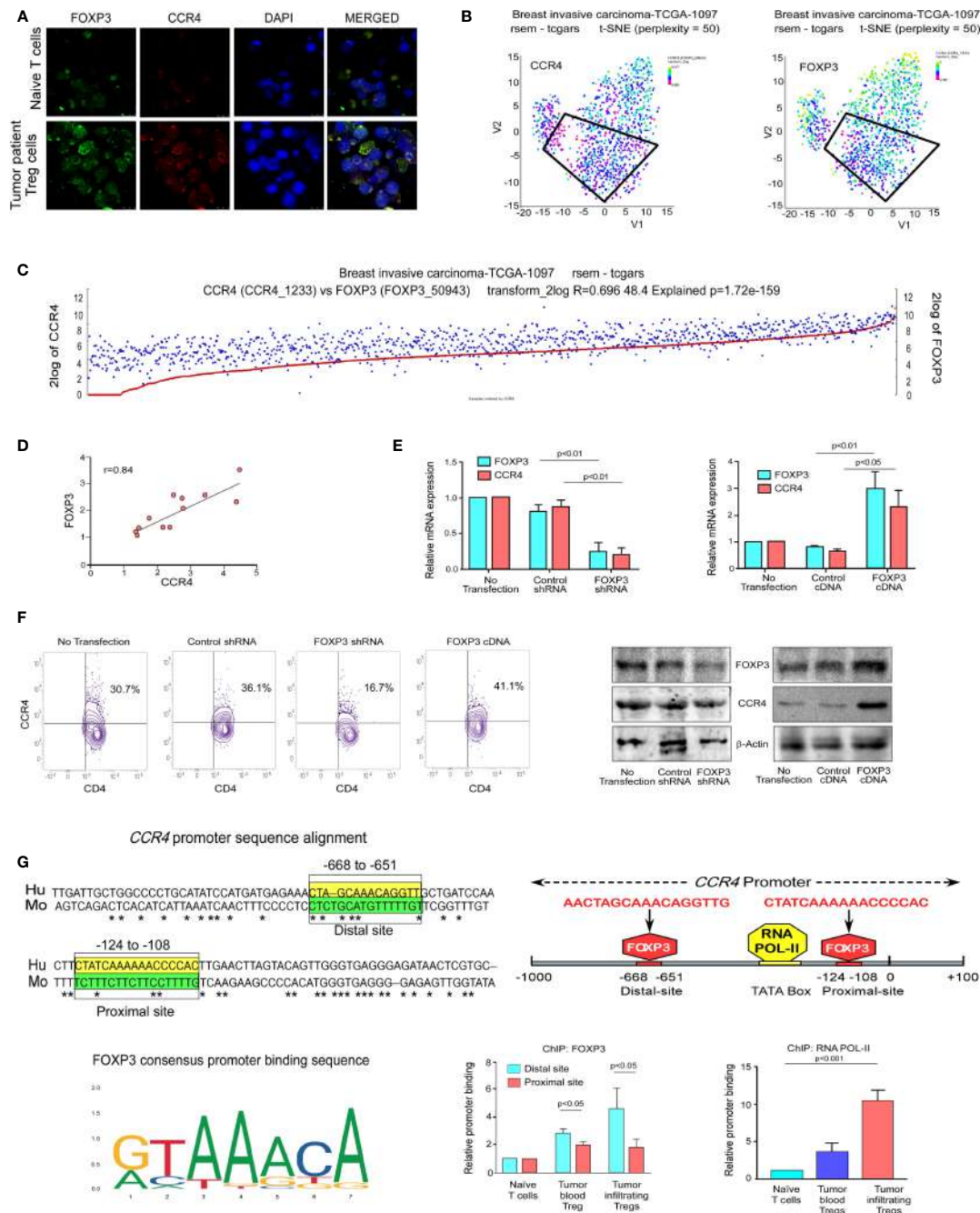
FIGURE 3 | FOXP3 binds at the *CCR4* promoter and regulates CCR4 expression in Treg cells. **(A)** The confocal microscopy data showing the expression of CCR4 and FOXP3 in naïve T cells and Treg cells of breast cancer patients. **(B)** the t-SNE plot of TCGA data from invasive breast carcinoma patients ($n = 1,097$), revealing CCR4 and FOXP3 expression levels. **(C)** FOXP3 and CCR4 correlation plot were derived from TCGA data of invasive breast cancer patients ($n = 1,097$). **(D)** Representative correlation coefficient plots depicting the relationship between CCR4 and FOXP3 in core breast tumor tissue taken from breast cancer patients at various stages ($n = 12$). **(E)** CCR4 and FOXP3 relative mRNA expression in FOXP3-ablated (left panel) and FOXP3-overexpressed (right panel) Tregs induced by shRNA or cDNA. **(F)** CCR4 protein expression in FOXP3-deficient and FOXP3-overexpressed Tregs (flow cytometry; left panel, Western blot; right panel). **(G)** The Fork-head DNA-binding site has been identified in a Clustal W depiction of multiple sequence alignment of the *CCR4* promoter between human and mouse (upper left panel). The consensus DNA-binding sequence for fork-heads has been discovered (obtained from Jasper) (lower left panel). On the *CCR4* promoter, there are two FOXP3-binding sites (Distal site: –668 bp to –651 bp and Proximal site: –124 bp to –108 bp) as well as an RNA POL-II binding region (TATA-Box) (upper right panel). The relative binding of FOXP3 at the *CCR4* promoter's distal (–668 bp to –651 bp) and proximal (–124 bp to –108 bp) sites are depicted graphically (lower middle panel). The relative binding of RNA POL-II to the TATA-box of the *CCR4* promoter has been graphically depicted (bottom right panel). GAPDH and β-actin were used as internal controls. The values are the mean ± SD of three sets of independent experiments.
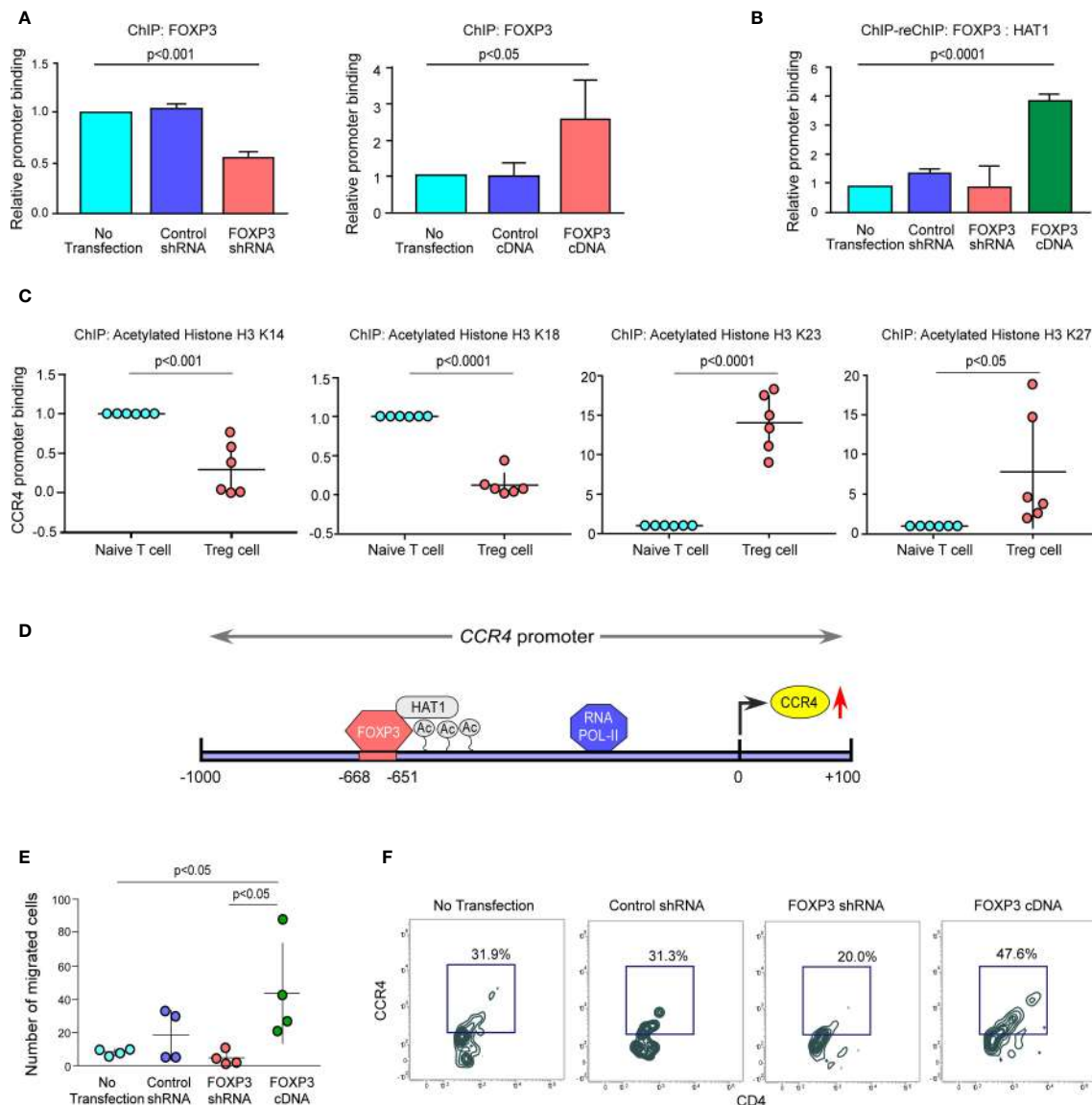
FIGURE 4 | The FOXP3/HAT1 axis epigenetically alters *CCR4* promoter to promote Treg infiltration in tumor site. **(A)** The relative binding of FOXP3 to its putative responsive elements on the *CCR4* promoter has been graphically depicted in FOXP3-ablated/-overexpressed Treg cells. **(B)** The binding of both FOXP3 and HAT1 to the *CCR4* promoter in FOXP3-ablated/-overexpressed Tregs was assessed using a ChIP-Re-ChIP assay, and the results are depicted graphically. **(C)** Relative permissive (K23 and K27) or repressive (K14 and K18) acetylation of histone-3 was determined using a ChIP assay and depicted graphically using site-specific antibodies. **(D)** Schematic illustration of the FOXP3-binding site on the *CCR4* promoter (–668 bp to –651 bp) with HAT1. **(E)** After 6 h, the number of FOXP3-ablated/overexpressed Treg cells in the lower chamber of the trans-well plate that migrated in response to recombinant CCL22 was counted and graphically displayed. **(F)** Flow cytometry was used to determine the percentage of FOXP3-ablated/overexpressed Treg cells that migrated in response to recombinant CCL22 in a trans-well plate (representative plot). The values are the mean ± SD of three sets of independent experiments.

confirm our hypothesis that FOXP3 regulates Treg infiltration in the tumor site. The number of migrating cells in the lower chamber was much higher in FOXP3-overexpressed cells than in FOXP3-ablated cells, according to the data in **Figure 4E**. Concurrently, CCR4 expression was found to be higher in the migrating Treg cells (**Figure 4F**). In conclusion, the FOXP3/HAT1 complex induces acetylation of the *CCR4* promoter in tumor Tregs, which regulates Treg infiltration in the TME.

FOXP3 Regulates CCR4 Expression and Infiltration of Tregs in the Tumor Site in the *In Vivo* Animal Model

We wanted to see if this phenomenon was true in the *in vivo* animal model because both breast cancer patient-derived Tregs and *ex vivo*-generated Treg cells showed a dependency of FOXP3 in the transcriptional regulation of *CCR4*, the key regulator of Treg infiltration in the TME. We employed

4T1-bearing breast carcinoma BALB/c mice and melanoma (B16/F10)-bearing C57/BL6 mice for this study. To genetically manipulate FOXP3 expression in mice, the mice were injected with lentivirus harboring Foxp3-shRNA or Foxp3-cDNA clones. The mice were monitored for 21 days after treatment. In both the breast carcinoma (**Figure 5A**) and melanoma (**Figure 6A**) models, FOXP3 ablation significantly reduced tumor volume and mass. The decrease in tumor size is accompanied by a decrease in CCR4$^+$ Treg generation both in the peripheral circulation (**Figures 5B**, **6B**) and at the tumor site (**Figures 5C**, **6C**), demonstrating that FOXP3 transcriptionally activates *CCR4* in both *in vitro* and *in vivo* settings. FOXP3 overexpression, on the other hand, enhanced tumor size (**Figures 5A**, **6A**) by increasing the percentage of CCR4$^+$ Tregs in the peripheral circulation (**Figures 5B**, **6B**) as well as at the tumor site (**Figures 5C**, **6C**).

DISCUSSION

Immune systems are essential for detecting cancer cells and activating efficient immune responses to eliminate them (43). Immune escape is a major hallmark of cancer growth, as it transforms from immunological surveillance (tumor eradication) to immune tolerance (tumor progression) (44). Researchers have long sought to manipulate immune cells to improve the efficacy of immune responses. Cancer immunotherapy involving the suppression of critical Treg-specific proteins like CD25 and the blockade of immune-checkpoint molecules like CTLA4 and PD1 has demonstrated great clinical results in a variety of cancers (45, 46). Long-term survival was observed in approximately 20% of patients treated with immune checkpoint inhibitors in a collective meta-analysis, whereas a large proportion of patients (nearly 80%) experience disease relapse after treatment, highlighting the role of Tregs as a stumbling block to successful immunotherapy. However, excessive reduction of the global pool of Tregs without cause can put the host system at risk of autoimmunity. As a result, detecting tumor-infiltrating Tregs and controlling them has become increasingly critical for effective immunotherapy that also reduces the danger of autoimmunity. Several preclinical and clinical investigations demonstrate that Treg infiltration in the TME interferes with treatments, prevents tumor-bearing hosts from developing antitumor immunity, and promotes tumor progression. As a result, contemporary cancer immunotherapy research has focused on preventing Tregs from infiltrating the TME to increase anti-tumor immunity (47).

Emerging evidence reveals that Treg compartmentalization and trafficking are tissue-specific, and that different chemokine receptors may play a role in Treg trafficking at specific tissue sites (24). Because CCR4 is a tumor-specific chemokine receptor, we examined its expression in Tregs from both the peripheral circulation (source) and the tumor site (destination) in breast cancer patients. CCR4$^+$ Tregs have a higher frequency distribution in the tumor site, but CCR4$^-$ Tregs dominate in the peripheral circulation, implying that Tregs that gain CCR4

expression in the peripheral circulation travel to the tumor site. This infiltrating CCR4$^+$ Treg expands in the tumor site, mounting the tumor immune escape. It is noteworthy that CCL22^{hi}/CCL17^{hi} breast tumor tissues are likewise CCR4^{hi}. In the TME, the core tumor cells as well as tumor-associated macrophages secrete high amounts of CCL22/CCL17. Finally, the CCR4-CCL22/CCL17 axis increases the accumulation of IL10-producing immunosuppressive Tregs in the TME.

Anti-CCR4 mAb could be an excellent therapy option for individuals with CCR4$^+$ neoplasms, as well as a novel strategy for treating cancers including HL, B-CLL, ovarian cancer, and EBV-associated disease, in which CCR4$^+$ Tregs prevent the host immune response to the tumor or virus-infected cells (48). Mogamulizumab is a humanized monoclonal antibody that targets CCR4 (36). It has been evaluated in humans for the treatment of CCR4$^+$ adult T cell leukemia/lymphoma that has relapsed or become refractory. This humanized antibody is also being looked into as a possible treatment for HTLV1–associated myelopathy (49). CCR4 is a promising target for antibody-based immunotherapy in cutaneous T-cell lymphoma (CTCL) and Tregs because of its high expression. In HL-bearing humanized mice, chimeric defucosylated anti-CCR4 mAb (KM2760) dramatically boosted the number of tumor-infiltrating NK cells that mediate ADCC and decreased the number of tumor-infiltrating FOXP3-positive Treg cells (50). The terminally differentiated and most suppressive effector Treg cells predominantly express CCR4 in both cancer tissues and peripheral blood and anti-CCR4 mAb treatment selectively depletes effector Treg cells and induces anti-tumor immunity (35). Anti-CCR4 mAb could be an appropriate treatment for a variety of malignancies, not only because it kills CCR4-expressing tumor cells directly, but also because it overcomes Treg cells' suppressive influence on the host immune response.

Despite the importance of CCR4 in Treg tumor invasion, there is very little information on its transcriptional regulation in tumor-associated Treg cells. However, few studies provide light on the transcriptional regulation of this chemokine receptor in different cancer types. For example, CCR4 is controlled by NFκB in colorectal cancer, promoting its metastasis (51). Fra-2 enhances CCR4 expression in adult T-cell leukemia (52), and HTLV-1 viral factor-generated GATA3 stimulates CCR4 expression in CD4$^+$ T cells (53). All of these studies have revealed that lineage-specific transcription factors play a critical role in the regulation of CCR4 expression.

FOXP3 carries out its diverse functions by regulating the transcription of its target genes. The t-SNE analysis of TCGA data from patients with breast invasive cancer also revealed a strong connection between CCR4 and FOXP3, which was further validated in our laboratory. Interestingly, it was observed that both human and murine *CCR4* promoters have consensus FOXP3-binding regions, and in naïve T cells, both the sites remain inaccessible due to their highly condensed heterochromatin state. FOXP3 recruits HAT1 at the distal FOXP3-binding site of *CCR4* promoter to convert highly condensed heterochromatin state to an open euchromatin state by permissive acetylation of lysine residues of histone-3. As a
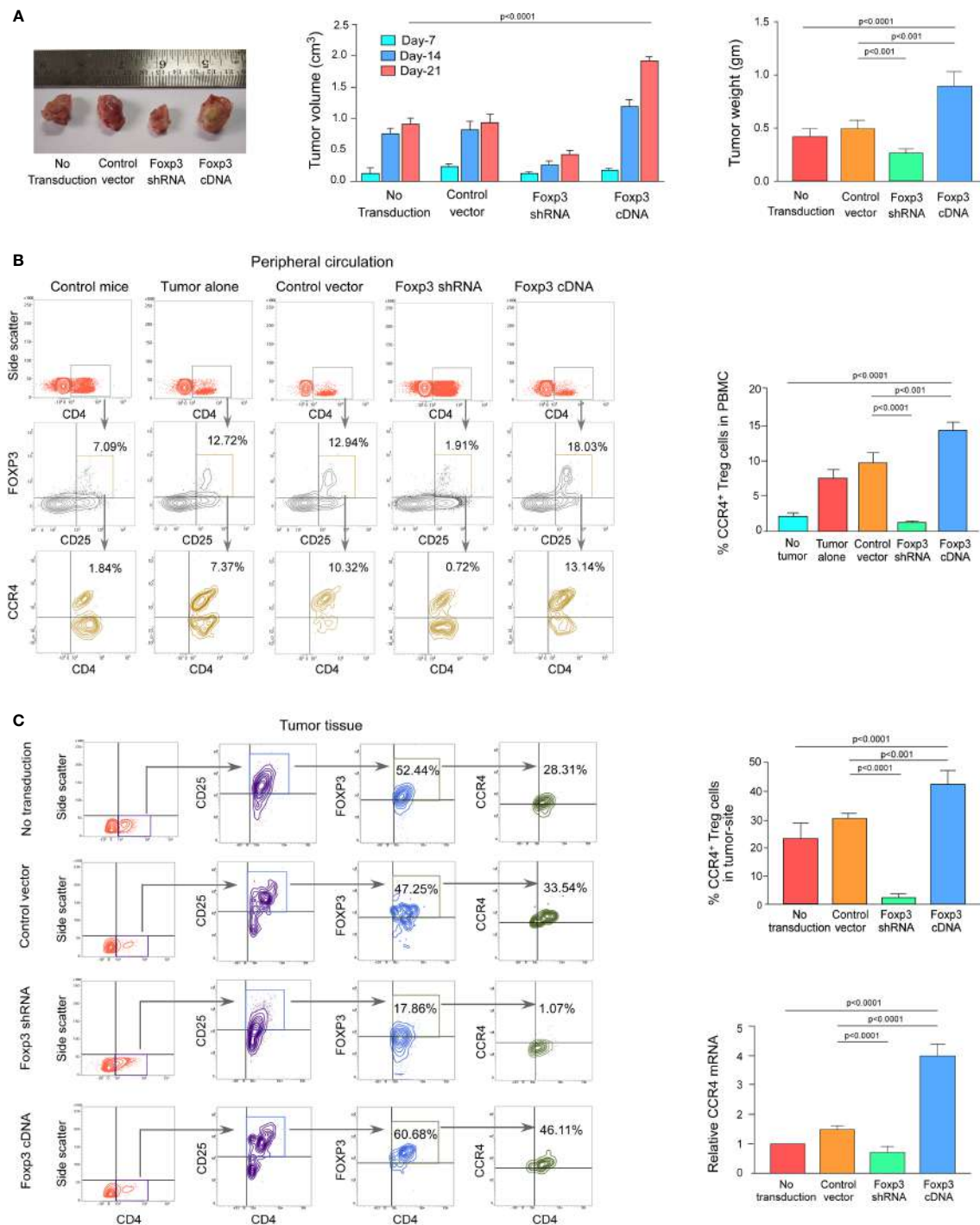
FIGURE 5 | FOXP3 regulates *Ccr4* transcription and infiltration of Tregs in mouse mammary carcinoma site. **(A)** In the tail veins of isogenic mammary cancer (4T1)-transplanted BALB/c mice, lentiviruses expressing Foxp3-shRNA or Foxp3-cDNA were injected (*n* = 6). Mice were sacrificed after 21 days, and the tumor was detached (left panel). The volume and weight of the tumor were measured and graphed (middle panel, right panel). CCR4 and FOXP3 positivity in Treg cells from **(B)** peripheral circulation and **(C)** tumor site were flow cytometrically analyzed (left panels) and graphically plotted (right panels). CCR4-mRNA transcript levels in tumor-infiltrating Tregs were measured using real-time PCR and graphed (lower right panel). As an internal control, GAPDH was used. The values are the mean ± SD of two sets of independent experiments performed in triplicate.
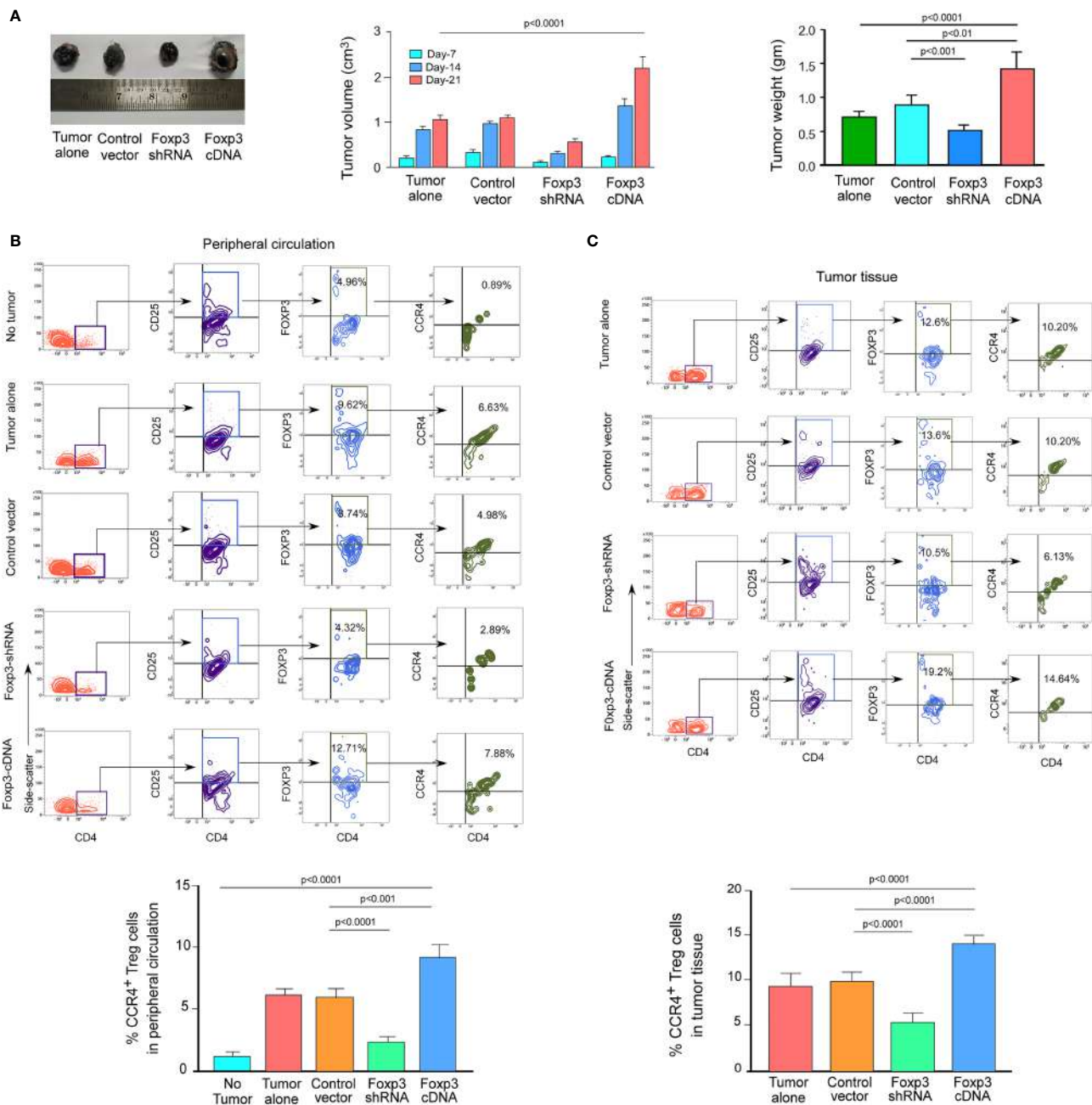
FIGURE 6 | FOXP3 regulates *Ccr4* transcription and infiltration of Tregs in mouse melanoma site. **(A)** Foxp3-shRNA or Foxp3-cDNA lentiviruses were injected into the tail veins of B16/F10 melanoma-transplanted C57/BL6 mice (*n* = 6). Mice were sacrificed after 21 days, and the tumor was detached (left panel). The volume and weight of the tumor were measured and graphed (middle panel, right panel). CCR4 and FOXP3 positivity in Tregs from **(B)** peripheral circulation and **(C)** tumor site were flow cytometrically analyzed (upper panels) and graphically plotted (lower panels). The values are the mean ± SD of two sets of independent experiments performed in triplicate.

result of this epigenetic landscape, FOXP3 and RNA POL-II get access at the distal-promoter region to transcribe *CCR4*.

In breast cancer patients, a high amount of TGFβ released by tumor cells, combined with sustained TCR-stimulation, increases the acquired expression of FOXP3 in CD4⁺CD25⁻ T cells, allowing them to develop into Treg cells. TGF/TCR

signaling also prevents DNA methyltransferase-1 from binding to the FOXP3 promoter, allowing FOXP3 expression to be preserved in Tregs (54). We also established that TGFβ-induced FOXP3 enhances *CCR4* transcription in Treg cells, making them amenable for tumor site infiltration (**Figure S3**). In both mammary carcinoma- and melanoma-bearing mice,

FIGURE 7 | FOXP3-transcribed CCR4 expression regulates Treg infiltration in tumor site. Left: CCR4^{+} Tregs are infiltrated in the tumor microenvironment in response to tumor-secreted CCL22/CCL17 to promote tumor immune escape. Right: FOXP3 in the association of HAT1 binds to *CCR4* promoter to epigenetically modify it for optimal transcription of *CCR4* gene.
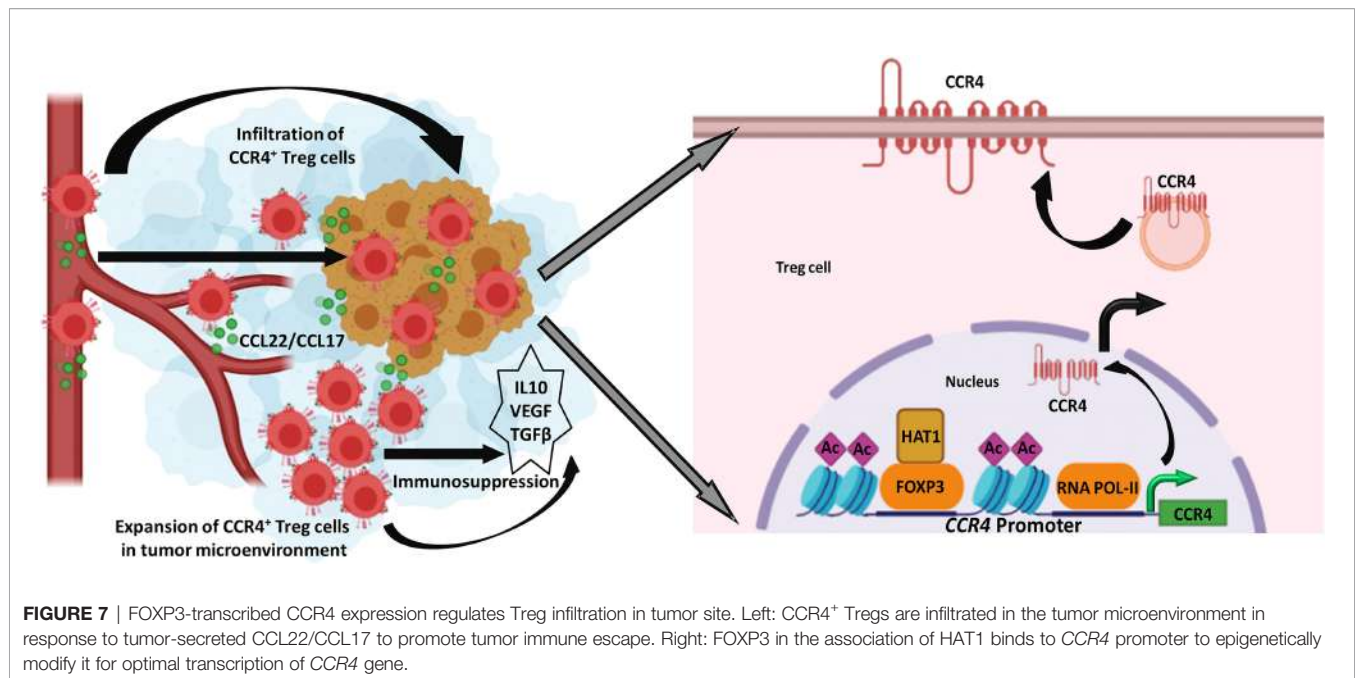
ablation of FOXP3 reduces the generation of CCR4^{+} Tregs and hence their infiltration into the tumor site. Reduced Treg infiltration resulted in an increase in anti-tumor immunity, which resulted in a reduction in tumor growth. The translational *in vivo* tumor model suggested that altering the expression of either CCR4 or FOXP3 in cancer patients could improve the efficacy of chemotherapy or immunotherapy.

Nowadays, the primary goal of cancer therapy is to limit tumor growth and increase treatment efficacy. The body's innate immune system works by recognizing and attacking "foreign" cells, but cancer cells disguise themselves to avoid detection by the host immune system. Tregs play a role in this scenario by suppressing both T-effector and T-cytotoxic cells, effectively making tumor cells "friendly." Immunotherapy's purpose is to help the host immune system recognize cancer cells as invaders and wage war on them, which can be done even more successfully by focusing on tumor cells' "friends". The tolerogenic environment of a cancer patient is created by Treg infiltration in the TME. When the balance between the proliferation and function of Treg and Teff cells is broken, tumor cells multiply more quickly.

Treg levels in the TME are linked to a cancer patient's poor prognosis and distant metastases. As a result, our research reveals that Treg infiltration in the TME is one of the major roadblocks to building anti-tumor immune escape. We reasoned that reducing CCR4 expression could aid in controlling these immunosuppressive pro-tumor Tregs and hence slow tumor growth. As a result, Treg infiltration interference in the TME has become a significant focus of research in recent years. Despite this, none of this research described how CCR4 expression in Treg cells is controlled. Our findings revealed a novel role for FOXP3 in the regulation of CCR4 expression in tumor-infiltrating Tregs (**Figure 7**) and gave a molecular insight

as to how immunosuppressive Tregs infiltrate into the TME, allowing us to disrupt the pathway implicated and increase cancer immunity.

DATA AVAILABILITY STATEMENT

The original contributions presented in the study are included in the article/**Supplementary Material**. Further inquiries can be directed to the corresponding author.

ETHICS STATEMENT

AUTHOR CONTRIBUTIONS

GS conceptualized and supervised the study and edited the manuscript. TS, SD, DC, SP, SB, AP, UB, SC, SM, and AG performed experiments and analyzed data. TS and SD wrote manuscript draft. DS provided support with clinical samples. SP and SB helped in bioinformatics data analysis. KJ provided support with animal experiments. All authors contributed to the article and approved the submitted version.

SUPPLEMENTARY MATERIAL

The Supplementary Material for this article can be found online at: https://www.frontiersin.org/articles/10.3389/fimmu.2022.740588/full#supplementary-material

REFERENCES

1. Wang M, Zhao J, Zhang L, Wei F, Lian Y, Wu Y, et al. Role of Tumor Microenvironment in Tumorigenesis. *J Cancer* (2017) 8(5):761–73. doi: 10.7150/jca.17648
2. Gonzalez H, Hagerling C, Werb Z. Roles of the Immune System in Cancer: From Tumor Initiation to Metastatic Progression. *Genes Dev* (2018) 32(19-20):1267–128. doi: 10.1101/gad.314617.118
3. Murdoch C, Muthana M, Coffelt SB, Lewis CE. The Role of Myeloid Cells in the Promotion of Tumor Angiogenesis. *Nat Rev Cancer* (2008) 8(8):618–31. doi: 10.1038/nrc2444
4. Darrasse-Jèze G, Podsypanina K. How Numbers, Nature, and Immune Status of Foxp3(+) Regulatory T-Cells Shape the Early Immunological Events in Tumor Development. *Front Immunol* (2013) 26:292. doi: 10.3389/fimmu.2013.00292
5. Sakaguchi S. Naturally Arising Foxp3-Expressing CD25+CD4+ Regulatory T Cells in Immunological Tolerance to Self and non-Self. *Nat Immunol* (2005) 6(4):345–52. doi: 10.1038/ni1178
6. Curotto de Lafaille MA, Lafaille JJ. Natural and Adaptive Foxp3+ Regulatory T Cells: More of the Same or a Division of Labor? *Immunity* (2009) 30(5):626–35. doi: 10.1016/j.immuni.2009.05.002
7. Workman CJ, Szymczak-Workman AL, Collison LW, Pillai MR, Vignali DAA. The Development and Function of Regulatory T Cells. *Cell Mol Life Sci CMLS* (2009) 66(16):2603–22. doi: 10.1007/s00018-009-0026-2
8. Shevach EM. Mechanisms of Foxp3+ T Regulatory Cell-Mediated Suppression. *Immunity* (2009) 30(5):636–45. doi: 10.1016/j.immuni.2009.04.010
9. Pandiyan P, Zheng L, Ishihara S, Reed J, Lenardo MJ. CD4+CD25+Foxp3+ Regulatory T Cells Induce Cytokine Deprivation-Mediated Apoptosis of Effector CD4+ T Cells. *Nat Immunol* (2007) 8(12):1353–62. doi: 10.1038/ni1536
10. Zheng Y, Josefowicz SZ, Kas A, Chu T-T, Gavin MA, Rudensky AY. Genome-Wide Analysis of Foxp3 Target Genes in Developing and Mature Regulatory T Cells. *Nature* (2007) 445(7130):936–40. doi: 10.1038/nature05563
11. Fontenot JD, Gavin MA, Rudensky AY. Foxp3 Programs the Development and Function of CD4+CD25+ Regulatory T Cells. *Nat Immunol* (2003) 4(4):330–6. doi: 10.1038/ni904
12. Strauss L, Bergmann C, Szczepanski M, Gooding W, Johnson JT, Whiteside TL. A Unique Subset of CD4+CD25highFoxp3+ T Cells Secreting Interleukin-10 and Transforming Growth Factor-Beta1 Mediates Suppression in the Tumor Microenvironment. *Clin Cancer Res Off J Am Assoc Cancer Res* (2007). doi: 10.1158/1078-0432.CCR-07-0472
13. Sarkar T, Dhar S, Sa G. Tumor-Infiltrating T-Regulatory Cells Adapt to Altered Metabolism to Promote Tumor-Immune Escape. *Curr Res Immunol* (2021) 2:132–41. doi: 10.1016/j.crimmu.2021.08.002
14. Ramsdell F. Foxp3 and Natural Regulatory T Cells: Key to a Cell Lineage? *Immunity* (2003) 19(2):165–8. doi: 10.1016/s1074-7613(03)00207-3
15. Garín MI, Chu C-C, Golshayan D, Cernuda-Morollón E, Wait R, Lechler RI. Galectin-1: A Key Effector of Regulation Mediated by CD4+CD25+ T Cells. *Blood* (2007) 109(5):2058–65. doi: 10.1182/blood-2006-04-016451
16. Borsellino G, Kleinewietfeld M, Di Mitri D, Sternjak A, Diamantini A, Giometto R, et al. Expression of Ectonucleotidase CD39 by Foxp3+ Treg Cells: Hydrolysis of Extracellular ATP and Immune Suppression. *Blood* (2007) 110(4):1225–32. doi: 10.1182/blood-2006-12-064527
17. Curiel TJ, Coukos G, Zou L, Alvarez X, Cheng P, Mottram P, et al. Specific Recruitment of Regulatory T Cells in Ovarian Carcinoma Fosters Immune Privilege and Predicts Reduced Survival. *Nat Med* (2004) 10:942–9. doi: 10.1038/nm1093
18. Ondondo B, Jones E, Godkin A, Gallimore A. Home Sweet Home: The Tumor Microenvironment as a Haven for Regulatory T Cells. *Front Immunol* (2013) 16:197. doi: 10.3389/fimmu.2013.00197
19. Mailloux AW, Young MRI. Regulatory T-Cell Trafficking: From Thymic Development to Tumor-Induced Immune Suppression. *Crit Rev Immunol* (2010) 30(5):435–47. doi: 10.1615/critrevimmunol.v30.i5.30
20. Le Y, Zhou Y, Iribarren P, Wang J. Chemokines and Chemokine Receptors: Their Manifold Roles in Homeostasis and Disease. *Cell Mol Immunol* (2004) 1(2):95–104.
21. Wang X, Lang M, Zhao T, Feng X, Zheng C, Huang C, et al. Cancer-FOXP3 Directly Activated CCL5 to Recruit FOXP3+Treg Cells in Pancreatic Ductal Adenocarcinoma. *Oncogene* (2017) 36(21):3048–58. doi: 10.1038/onc.2016.458
22. Redjimi N, Raffin C, Raimbaud I, Pignon P, Matsuzaki J, Odunsi K, et al. CXCR3+ T Regulatory Cells Selectively Accumulate in Human Ovarian Carcinomas to Limit Type I Immunity. *Cancer Res* (2012) 72(17):4351–436. doi: 10.1158/0008-5472.CAN-12-0579
23. Halvorsen EC, Hamilton MJ, Young A, Wadsworth BJ, LePard NE, Lee HN, et al. Maraviroc Decreases CCL8-Mediated Migration of CCR5(+) Regulatory T Cells and Reduces Metastatic Tumor Growth in the Lungs. *Oncoimmunology* (2016) 5(6):e1150398. doi: 10.1080/2162402X.2016.1150398
24. Wei S, Kryczek I, Zou W. Regulatory T-Cell Compartmentalization and Trafficking. *Blood* (2006) 108(2):426–31. doi: 10.1182/blood-2006-01-0177
25. Iellem A, Mariani M, Lang R, Recalde H, Panina-Bordignon P, Sinigaglia F, et al. Unique Chemotactic Response Profile and Specific Expression of Chemokine Receptors CCR4 and CCR8 by CD4(+)CD25(+) Regulatory T Cells. *J Exp Med* (2001) 194(6):847–53. doi: 10.1084/jem.194.6.847
26. Imai T, Nagira M, Takagi S, Kakizaki M, Nishimura M, Wang J, et al. Selective Recruitment of CCR4-Bearing Th2 Cells Toward Antigen-Presenting Cells by the CC Chemokines Thymus and Activation-Regulated Chemokine and Macrophage-Derived Chemokine. *Int Immunol* (1999) 11(1):81–8. doi: 10.1093/intimm/11.1.81
27. Imai T, Baba M, Nishimura M, Kakizaki M, Takagi S, Yoshie O. The T Cell-Directed CC Chemokine TARC Is a Highly Specific Biological Ligand for CC Chemokine Receptor 4. *J Biol Chem* (1997) 272(23):15036–42. doi: 10.1074/jbc.272.23.15036
28. Imai T, Chantry D, Raport CJ, Wood CL, Nishimura M, Godiska R, et al. Macrophage-Derived Chemokine Is a Functional Ligand for the CC Chemokine Receptor 4. *J Biol Chem* (1998) 273(3):1764–8. doi: 10.1074/jbc.273.3.1764
29. Vulcano M, Albanesi C, Stoppacciaro A, Bagnati R, D'Amico G, Struyf S, et al. Dendritic Cells as a Major Source of Macrophage-Derived Chemokine/CCL22 *In Vitro* and In Vivo. *Eur J Immunol* (2001) 31(3):812–22. doi: 10.1002/1521-4141(200103)31:3<812::aid-immu812>3.0.co;2-l
30. Gobert M, Treilleux I, Bendriss-Vermare N, Bachelot T, Goddard-Leon S, Arfi V, et al. Regulatory T Cells Recruited Through CCL22/CCR4 Are Selectively Activated in Lymphoid Infiltrates Surrounding Primary Breast Tumors and Lead to an Adverse Clinical Outcome. *Cancer Res* (2009) 69(5):2000–9. doi: 10.1158/0008-5472.CAN-08-2360

31. Ishida T, Ishii T, Inagaki A, Yano H, Komatsu H, Iida S, et al. Specific Recruitment of CC Chemokine Receptor 4-Positive Regulatory T Cells in Hodgkin Lymphoma Fosters Immune Privilege. *Cancer Res* (2006) 66 (11):5716–22. doi: 10.1158/0008-5472.CAN-06-0261

32. Mizukami Y, Kono K, Kawaguchi Y, Akaike H, Kamimura K, Sugai H, et al. CCL17 and CCL22 Chemokines Within Tumor Microenvironment Are Related to Accumulation of Foxp3+ Regulatory T Cells in Gastric Cancer. *Int J Cancer* (2008) 122(10):2286–93. doi: 10.1002/ijc.23392

33. Sakaguchi S, Miyara M, Costantino CM, Hafler DA. FOXP3+ Regulatory T Cells in the Human Immune System. *Nat Rev Immunol* (2010) 10(7):490–500. doi: 10.1038/nri2785

34. Saleh R, Elkord E. Treg-Mediated Acquired Resistance to Immune Checkpoint Inhibitors. *Cancer Lett* (2019) 457:168–79. doi: 10.1016/j.canlet.2019.05.003

35. Sugiyama D, Nishikawa H, Maeda Y, Nishioka M, Tanemura A, Katayama I, et al. Anti-CCR4 Mab Selectively Depletes Effector-Type Foxp3+CD4+ Regulatory T Cells, Evoking Antitumor Immune Responses in Humans. *Proc Natl Acad Sci USA* (2013) 110(44):17945–50. doi: 10.1073/pnas.1316796110

36. Moore DC, Elmes JB, Shibu PA, Larck C, Park SI. Mogamulizumab: An Anti-CC Chemokine Receptor 4 Antibody for T-Cell Lymphomas. *Ann Pharmacother* (2020) 54(4):371–9. doi: 10.1177/1060028019884863

37. Marson A, Kretschmer K, Frampton GM, Jacobsen ES, Polansky JK, MacIsaac KD, et al. Foxp3 Occupancy and Regulation of Key Target Genes During T-Cell Stimulation. *Nature* (2007) 445(7130):931–5. doi: 10.1038/nature05478

38. Roy D, Bose S, Pati S, Guin A, Banerjee K, Saha S, et al. GFI1/HDAC1-Axis Differentially Regulates Immunosuppressive CD73 in Human Tumor-Associated FOXP3+ Th17 and Inflammation-Linked Th17 Cells. *Eur J Immunol* (2021) 51(5):1206–17. doi: 10.1002/eji.202048892

39. Chakraborty S, Panda AK, Bose S, Roy D, Kajal K, Guha D, et al. Transcriptional Regulation of FOXP3 Requires Integrated Activation of Both Promoter and CNS Regions in Tumor-Induced CD8+ Treg Cells. *Sci Rep* (2017). doi: 10.1038/s41598-017-01788-z

40. Saha T, Guha D, Manna A, Panda AK, Bhat J, Chatterjee S, et al. G-Actin Guides P53 Nuclear Transport: Potential Contribution of Monomeric Actin in Altered Localization of Mutant P53. *Sci Rep* (2016) 6:32626. doi: 10.1038/srep32626

41. Kajal K, Bose S, Panda AK, Chakraborty D, Chakraborty S, Pati S, et al. Transcriptional Regulation of VEGFA Expression in T-Regulatory Cells From Breast Cancer Patients. *Cancer Immunol Immunother* (2021) 70(7):1877–91. doi: 10.1007/s00262-020-02808-0

42. Kajal K, Panda AK, Bhat J, Chakraborty D, Bose S, Bhattacharjee P, et al. Andrographolide Binds to ATP-Binding Pocket of VEGFR2 to Impede VEGFA-Mediated Tumor-Angiogenesis. *Sci Rep* (2019) 9(1):4073. doi: 10.1038/s41598-019-40626-2

43. Grivennikov SI, Greten FR, Karin M. Immunity, Inflammation, and Cancer. *Cell* (2010) 140(6):883–99. doi: 10.1016/j.cell.2010.01.025

44. Tang S, Ning Q, Yang L, Mo Z, Tang S. Mechanisms of Immune Escape in the Cancer Immune Cycle. *Int Immunopharmacol* (2020) 86:106700. doi: 10.1016/j.intimp.2020.106700

45. Hodi FS, O'Day SJ, McDermott DF, Weber RW, Sosman JA, Haanen JB, et al. Improved Survival With Ipilimumab in Patients With Metastatic Melanoma. *N Engl J Med* (2010) 363(8):711–23. doi: 10.1056/NEJMoa1003466

46. Topalian SL, Hodi FS, Brahmer JR, Gettinger SN, Smith DC, McDermott DF, et al. Safety, Activity, and Immune Correlates of Anti-PD-1 Antibody in Cancer. *N Engl J Med* (2012) 366(26):2443–54. doi: 10.1056/NEJMoa1200690

47. Ishida T, Ueda R. CCR4 as a Novel Molecular Target for Immunotherapy of Cancer. *Cancer Sci* (2006) 97(11):1139–46. doi: 10.1111/j.1349-7006.2006.00307.x

48. Ishida T, Utsunomiya A, Iida S, Inagaki H, Takatsuka Y, Kusumoto S, et al. Clinical Significance of CCR4 Expression in Adult T-Cell Leukemia/Lymphoma: Its Close Association With Skin Involvement and Unfavorable Outcome. *Clin Cancer Res Off J Am Assoc Cancer Res* (2003) 9:3625–34.

49. Sato T, Coler-Reilly A, Yagishita N, Araya N, Inoue E, Furuta R, et al. Mogamulizumab (Anti-CCR4) in HTLV-1-Associated Myelopathy. *New Engl J Med* (2018) 378(6):529–38. doi: 10.1056/NEJMoa1704827

50. Ishida T, Ishii T, Inagaki A, Yano H, Kusumoto S, Ri M, et al. The CCR4 as a Novel-Specific Molecular Target for Immunotherapy in Hodgkin Lymphoma. *Leukemia* (2006) 20(12):2162–8. doi: 10.1038/sj.leu.2404415

51. Ou B, Zhao J, Guan S, Feng H, Wangpu X, Zhu C, et al. CCR4 Promotes Metastasis *via* ERK/NF-κb/MMP13 Pathway and Acts Downstream of TNF-α in Colorectal Cancer. *Oncotarget* (2016) 7(30):47637–49. doi: 10.18632/oncotarget.10256

52. Nakayama T, Hieshima K, Arao T, Jin Z, Nagakubo D, Shirakawa A-K, et al. Aberrant Expression of Fra-2 Promotes CCR4 Expression and Cell Proliferation in Adult T-Cell Leukemia. *Oncogene* (2008) 27:3221–32. doi: 10.1038/sj.onc.1210984

53. Sugata K, Yasunaga J-I, Kinosada H, Mitobe Y, Furuta R, Mahgoub M, et al. HTLV-1 Viral Factor HBZ Induces CCR4 to Promote T-Cell Migration and Proliferation. *Cancer Res* (2016) 76(17):5068–79. doi: 10.1158/0008-5472.CAN-16-0361

54. Josefowicz SZ, Wilson CB, Rudensky AY. Cutting Edge: TCR Stimulation is Sufficient for Induction of Foxp3 Expression in the Absence of DNA Methyltransferase 1. *J Immunol Baltim Md 1950* (2009) 182(11):6648–52. doi: 10.4049/jimmunol.0803320